

JUL 16 1982

AEDC-TR-81-29

C-2



# High-Resolution Spectral Absorption in the Short Wavelength Wing of the 2.7- $\mu$ m Water Band at 1,000K

L. M. Peterson  
Environmental Research Institute of Michigan  
Consultant to  
Sverdrup Technology, Inc.

April 1982

Final Report for Period March 4 — September 15, 1980

Property of U. S. Air Force  
ALDO LIBRARY  
F40866-81-0-0004

Approved for public release; distribution unlimited.

**ARNOLD ENGINEERING DEVELOPMENT CENTER  
ARNOLD AIR FORCE STATION, TENNESSEE  
AIR FORCE SYSTEMS COMMAND  
UNITED STATES AIR FORCE**

## NOTICES

When U. S. Government drawings, specifications, or other data are used for any purpose other than a definitely related Government procurement operation, the Government thereby incurs no responsibility nor any obligation whatsoever, and the fact that the government may have formulated, furnished, or in any way supplied the said drawings, specifications, or other data, is not to be regarded by implication or otherwise, or in any manner licensing the holder or any other person or corporation, or conveying any rights or permission to manufacture, use, or sell any patented invention that may in any way be related thereto.

Qualified users may obtain copies of this report from the Defense Technical Information Center.

References to named commercial products in this report are not to be considered in any sense as an endorsement of the product by the United States Air Force or the Government.

This final report was submitted by Environmental Research Institute of Michigan, under subcontract (P.O. OX-681-A) to Sverdrup Technology, Inc., operating contractor of the engine testing facilities at the Arnold Engineering Development Center, AFSC, Arnold Air Force Station, Tennessee. Dr. C. C. Limbaugh was the Sverdrup Technology contract monitor; Air Force project managers were Dr. H. E. Scott and Maj. N. J. Cochrane.

This report has been reviewed by the Office of Public Affairs (PA) and is releasable to the National Technical Information Service (NTIS). At NTIS, it will be available to the general public, including foreign nations.

## APPROVAL STATEMENT

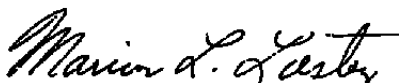
This report has been reviewed and approved



NORMAN J. COCHRANE, Major, USAF  
Directorate of Technology  
Deputy for Operations

Approved for publication:

FOR THE COMMANDER



MARION L. LASTER  
Director of Technology  
Deputy for Operations

## UNCLASSIFIED

SECURITY CLASSIFICATION OF THIS PAGE (When Data Entered)

REPORT DOCUMENTATION PAGE		READ INSTRUCTIONS BEFORE COMPLETING FORM
1. REPORT NUMBER AEDC-TR-81-29	2. GOVT ACCESSION NO.	3. RECIPIENT'S CATALOG NUMBER
4. TITLE (and Subtitle) HIGH-RESOLUTION SPECTRAL ABSORPTION IN THE SHORT WAVELENGTH WING OF THE 2.7-um WATER BAND AT 1,000K		5. TYPE OF REPORT & PERIOD COVERED Final - 4 March - 15 September 1980
7. AUTHOR(s) L. M. Peterson, Environmental Research Institute of Michigan		6. PERFORMING ORG. REPORT NUMBER 149100-1-T
9. PERFORMING ORGANIZATION NAME AND ADDRESS Environmental Research Institute of Michigan Ann Arbor, MI 48107		8. CONTRACT OR GRANT NUMBER(s) P.O. OX-681-A
11. CONTROLLING OFFICE NAME AND ADDRESS Arnold Engineering Development Center/DOS Air Force Systems Command Arnold Air Force Station, TN 37389		10. PROGRAM ELEMENT PROJECT, TASK AREA & WORK UNIT NUMBERS Program Element 65807F
14. MONITORING AGENCY NAME & ADDRESS (if different from Controlling Office)		12. REPORT DATE April 1982
		13. NUMBER OF PAGES 73
		15. SECURITY CLASS. (of this report) UNCLASSIFIED
		15a. DECLASSIFICATION/DOWNGRADING SCHEDULE N/A
16. DISTRIBUTION STATEMENT (of this Report)  Approved for public release; distribution unlimited.		
17. DISTRIBUTION STATEMENT (of the abstract entered in Block 20, if different from Report)		
18. SUPPLEMENTARY NOTES  Available in Defense Technical Information Center (DTIC).		
19. KEY WORDS (Continue on reverse side if necessary and identify by block number)  spectrometers                      absorption spectra spectra                              hydrogen fluoride water vapor high resolution		
20. ABSTRACT (Continue on reverse side if necessary and identify by block number)  High-temperature water vapor absorption measurements taken by Environmental Research Institute of Michigan in 1978 have been reduced and compared with computer-generated spectra based upon the Air Force Geophysics Laboratory line tabulation. The latter tabulation failed to predict numerous spectral lines, or, in many cases, did not predict them accurately. Although the scope of this particular effort allowed only a brief analysis of a few		

UNCLASSIFIED

SECURITY CLASSIFICATION OF THIS PAGE(When Data Entered)

20. ABSTRACT (CONTINUED)

lines in a selected spectral interval, the analysis did show the data to be useful in providing values of line strength, line width (self-broadened), and lower state energy.

UNCLASSIFIED

SECURITY CLASSIFICATION OF THIS PAGE(When Data Entered)

## **PREFACE**

The work reported herein was conducted by the Environmental Research Institute of Michigan (ERIM) at the request of Sverdrup Technology, Inc., for the Arnold Engineering Development Center (AEDC), Air Force Systems Command (AFSC). The results of the analysis reported here were obtained by ERIM under subcontract (P.O. OX-681-A) to Sverdrup Technology, Inc. (Project No. P32M-12), operating contractor of the engine test facilities at the AEDC. The Air Force Project Managers were Dr. H. E. Scott and Maj. N. J. Cochrane. The Sverdrup Technology contract monitor was Dr. C. C. Limbaugh. The author of this report is Dr. Lauren Peterson, and the manuscript was received for publication on October 21, 1981. The reproducibles used in the reproduction of this report were supplied by the authors.

## CONTENTS

	<u>Page</u>
1.0 INTRODUCTION .....	05
2.0 APPARATUS .....	06
3.0 PROCEDURE .....	09
3.1 Gas Handling .....	09
3.2 Spectrometer Calibration .....	10
4.0 RESULTS .....	12
4.1 Absorptance Spectra .....	12
4.2 Line Parameters Determination .....	14
5.0 CONCLUDING REMARKS .....	20
REFERENCES .....	21

## ILLUSTRATIONS

<u>Figure</u>	<u>Page</u>
1. Schematic of the Experimental System for High-Resolution Studies .....	06
2. High-Temperature Absorption Cell Using Kovar® -Sapphire Window Assemblies .....	07
3. Block Diagram of Digital Data Collection System .....	08
4. Gas Handling System for Generating and Measuring Water Vapor at Near-Atmospheric Pressures .....	10
5. Measured Absorptance Spectra Appear at the Top and Corresponding Computer Generated Spectra Appear at the Bottom .....	14
6. Measured Hot Cell Radiance (Upper) and Hot-Through-Cold Radiance (Lower) .....	20

## TABLES

1. Observed and Calculated Wave Numbers of the Rotation Lines in the (0-1) and (0-2) Bands of HF .....	11
2. ERIM 2.5- $\mu$ m Water Vapor Data .....	13
3. Spectral Line Parameters .....	19

## APPENDIXES

A. Water Vapor Spectra from 3,930 to 4,235 $\text{cm}^{-1}$ .....	23
B. IR Spectra Deconvolution .....	65

## 1.0 INTRODUCTION

In 1977, under Defense Advanced Research Projects Agency (DARPA) funding, Peterson and Doak of the Environmental Research Institute of Michigan (ERIM) conducted spectral measurements in the long wavelength wing of the 2.7- $\mu\text{m}$  water band using a 15-cm absorption cell at temperatures to 1,000K. Absorptance spectra of pure water vapor (no foreign gas broadening) were obtained at seven different temperatures from 500 to 1,000K using a 1.8-m grating spectrometer operated in double pass to achieve a resolution of 0.07  $\text{cm}^{-1}$ . The observed line spectra from 2,900 to 3,800  $\text{cm}^{-1}$  were compared with the Air Force Geophysics Laboratory (AFGL) atmospheric absorption line compilation, (Ref. 1). Agreement was good near band center but poor in the far wing regions, showing the compilation to be deficient in representing "hot" lines of water vapor.

The scope of the DARPA program did not include measurement in the short wavelength wing of the 2.7- $\mu\text{m}$  water band; however, ERIM performed these measurements under its own funding for completeness. Measurements at two temperatures, 704K and 1,002K, and pressures of 280 torr and 414 torr, respectively, were obtained, although no background scans were performed. The resolution in this spectral region around 2.5- $\mu\text{m}$  or 4,000  $\text{cm}^{-1}$  was 0.10  $\text{cm}^{-1}$ , as extrapolated from the instrument profile measurements around 3,000  $\text{cm}^{-1}$ .

These absorptance measurements allow the following determinations:

1. Line strength — from the magnitude of the absorption intensity.
2. Line width (self-broadened) — from the deconvolved spectral half-width-at-half-intensity, and
3. Lower state energy — from the temperature dependence of the line strength determination.

This report summarizes the analysis of the aforementioned raw data. Specifically, this analysis involved:

1. reducing the raw data tapes to absolute absorptance versus wave number;
2. generating a simulated water vapor spectrum based upon the AFGL line compilation (Ref. 1) and comparing it with the measured spectra; and
3. assessing the deficiency of the line compilation and providing a preliminary estimate of line strengths, widths, and lower state energies for lines in a selected spectral region.

The work reported herein was conducted at ERIM at the request of Sverdrup Technology, Inc., for the Arnold Engineering Development Center (AEDC), Air Force Systems Command (AFSC). A magnetic tape of the reduced data (IBM 370/165 compatible) has been delivered to Arnold Engineering Development Center.

## 2.0 APPARATUS

The optical system used for high-resolution spectral measurements is shown schematically in Fig. 1. The basic instrument is a Jarrell-Ash 1.83-m scanning vacuum spectrometer of Ebert-Fastie design using a 190- by 135-mm replica grating, double passed for improved resolution. The effective aperture of the instrument is  $f/11$ ; auxiliary vacuum optics were constructed to couple the source, absorption cell, and detector into the optical system. A quartz-halogen lamp with a color temperature of 3,100K is used as a source of radiant energy.

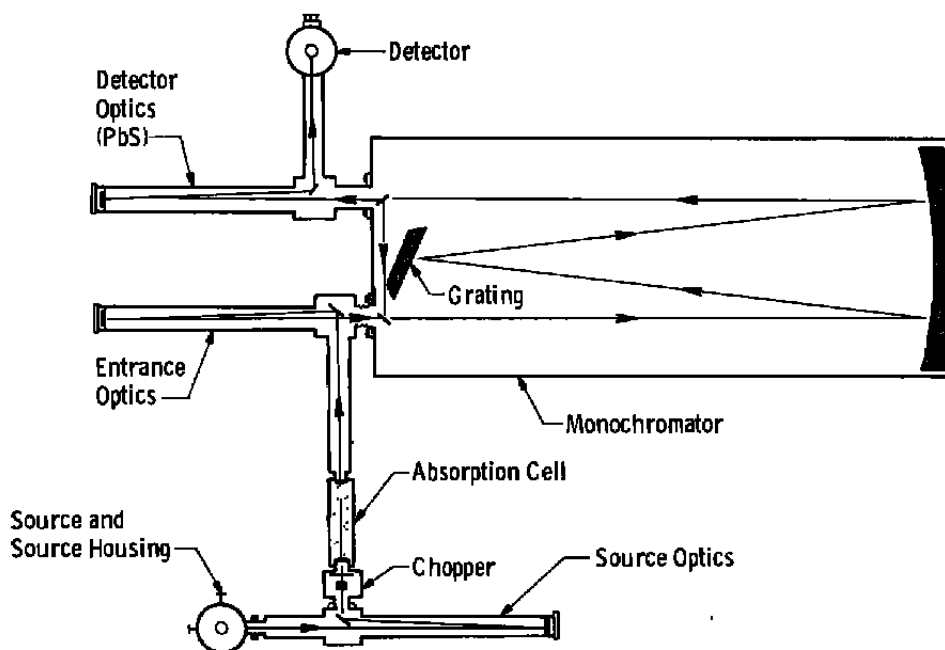


**Figure 1. Schematic of the experimental system for high-resolution studies.**



To ensure that the beam remains in the gas absorption cell, a speed of  $f/20$  was chosen for the entrance optics. Since the spectrometer requires an  $f/11$  beam to fill the grating properly, vacuum coupling optics are used to match the  $f/20$  beam with the instrument. For high-temperature spectral measurements (700K to 1,100K) a stainless steel cell was fabricated which uses commercial Kovar® -Sapphire window assemblies. As shown in Fig. 2, the cell is mounted inside a thin wall stainless steel tube so a vacuum can be maintained around the absorption cell itself. This is an important design consideration since, in an oxidizing atmosphere, the cell cannot withstand temperatures above 700K without danger of oxidizing the copper brazing which seals the windows to the Kovar flanges.

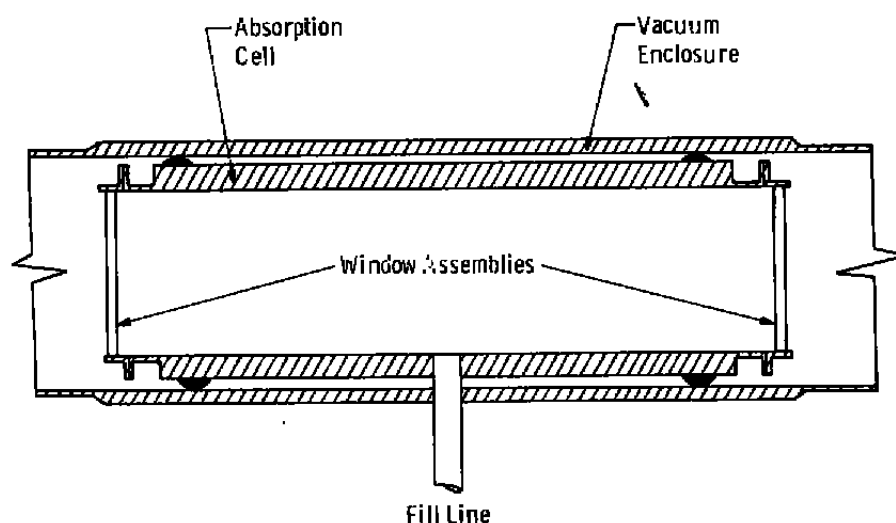


**Figure 2. High-temperature absorption cell using Kovar® -sapphire window assemblies.**

The detector used in the  $2.7\text{-}\mu\text{m}$  band is a PbS photoconductive cell with a measured  $D^*$  of  $2.0 \times 10^{11} \text{ cm Hz}^{1/2}\text{w}^{-1}$ . The detector chip is mounted in a liquid nitrogen dewar with an antireflection-coated germanium window. The short wavelength cutoff of this window acts as an order-storing filter for the spectrometer. Since the  $D^*$  measurements indicated an optimum operation temperature of  $-90^\circ\text{C}$  for this detector, the detector can be cooled with liquid ethane, which has a boiling point of  $-88.6^\circ\text{C}$ , to obtain a maximum signal-to-noise ratio. However, for the sake of convenience, and because the signal-to-noise ratio of the system was very good, liquid nitrogen was used for cooling. By using  $50\text{-}\mu\text{m}$  entrance and exit slit widths and integration time of 1.0 sec, a signal-to-noise ratio on the order of 200 was obtained, even at  $\text{LN}_2$  temperature.

Signals from the detector and its preamplifier were synchronously detected and amplified by a Princeton Applied Research lock-in amplifier set to the chopping frequency of 510 Hz. The output of this amplifier was displayed on a chart recorder and stored digitally on magnetic tape cassettes using the data acquisition system shown in Fig. 3.

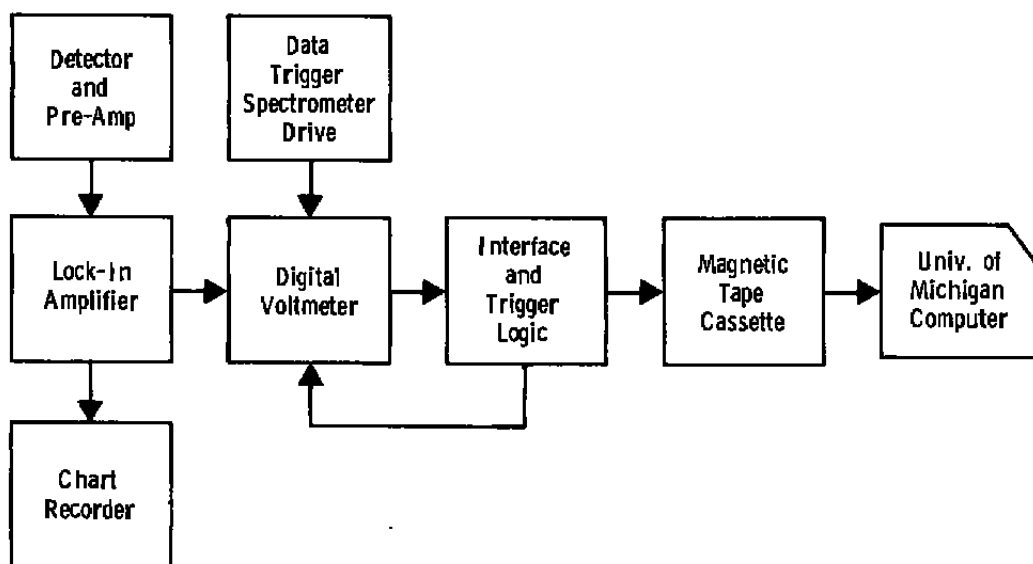


**Figure 3. Block diagram of digital data collection system.**

To maintain a wavelength base for the digitized data, the data coupler was triggered by pulses from a slotted-disc-photocell assembly on the spectrometer drive system, causing data points to be recorded at equal wavelength intervals\* on the magnetic tape cassette. As a check for recording errors, a second pulse was generated by this assembly every 20 data points, and a minus sign was recorded with the data. The computer program used to reduce the data determined if the proper number of data points was recorded between these markers and, if an error occurs, the operator is informed and the data reduction terminated. In addition to data reduction codes, codes have been developed to generate synthetic spectra using either band model or line-by-line techniques. These codes can be used to compare predicted spectra with those observed experimentally and have limited ranges of applicability determined by the accuracy of the tabulations they employ.

---

\*The majority of the data in this program were taken at a scan of  $17 \text{ \AA}/\text{min}$  ( $2 \text{ cm}^{-1}/\text{min}$  at  $3,450 \text{ cm}^{-1}$ ) and a recording rate of 12 data points per  $\text{\AA}$  (100 data points per  $\text{cm}^{-1}$  at  $3,450 \text{ cm}^{-1}$ ).

### 3.0 PROCEDURE

#### 3.1 GAS HANDLING

Since the vapor pressure of water at room temperature is only about 20 torr, a liquid water reservoir at a temperature from 66 to 87°C must be provided to achieve the desired vapor pressures. Since water will condense in any cool portion of the system, the plumbing between the water reservoir and hot cell must be maintained at a temperature approaching 100°C. If the water source is adequately pure and if its temperature is accurately measured, the vapor pressure may be obtained from tables (Ref. 2). In this temperature range, however, the vapor pressure of water changes rapidly with temperature, about 10 torr per °C, such that the thermometric technique needs to be accurate to about 0.1°C.

The gas handling system is shown in Fig. 4. Doubly distilled water is placed in the flask and then the flask is surrounded with a heat blanket. A mercury thermometer is partially immersed in the water, supported above the flask bottom by a hollow glass pedestal, and projecting upward through a ground glass joint into a column for viewing. The column is wrapped in heating tape, except for a long vertical strip which may be removed for viewing. The connective plumbing and packless (bellows type) valves are all stainless steel and are wrapped in insulation, heater tape, and insulation. Although not absolutely necessary, a pressure gauge may be used to verify that the water pressure is indeed as determined by the temperature of the water reservoir and that cool portions in the plumbing (such as at the valves) are not suppressing the pressure. A mercury manometer was available (a digital capacitive manometer — Baratron, Inc. — would be desirable) and was used in the system, along with a hot mercury vapor lock which kept the water vapor from the cool manometer. The vapor lock was kept warm using a 95°C water bath with a dipstick heater. A small cylinder of hydrogen fluoride (HF) was used sparingly for calibration purposes, and a liquid nitrogen cold trap, diffusion pump, and fore pump were used to evacuate the system. The high volume of water vapor used through repeated filling and flushing of the cell was hard on the fore pump, requiring frequent oil replacement and causing catastrophic failure of a pump on one occasion.

A desired water vapor pressure was obtained by pumping periodically on the water flask, applying power to the heating blanket surrounding the flask, and then allowing it to equilibrate overnight. The cell, also coming to temperature overnight, was then filled several times and evacuated. The final fill was obtained slowly, with the valve to the vapor lock open and slowly bleeding atmospheric air into the region between vapor lock and manometer such that the vapor lock was always near a balanced condition. Once full pressure was obtained, the vapor lock was precisely balanced, the temperature of the water reservoir was read, and its corresponding vapor pressure was compared with the manometer

reading. During a scan, the valve to the water reservoir was closed, but the pressure was constantly monitored to be sure there were no significant fluctuations.

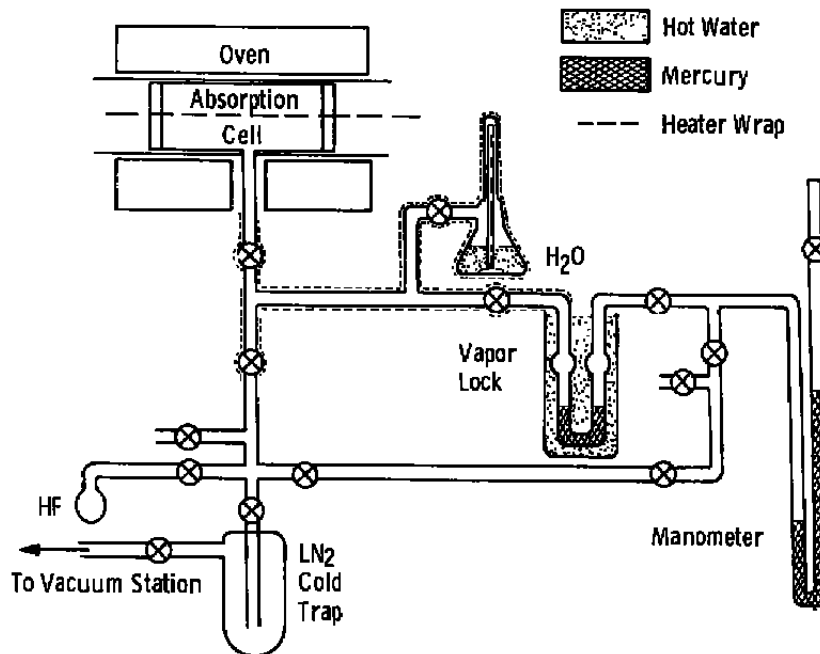


**Figure 4. Gas handling system for generating and measuring water vapor at near-atmospheric pressures.**

### 3.2 SPECTROMETER CALIBRATION

Wavelength calibration of the spectrometer was determined using the well-documented lines of the P-branch of HF gas (Ref. 3) presented in Table 1. Spectrometer drum numbers were recorded for the HF lines P(4) through P(10) over the wavelength region 2.64 - 2.86  $\mu\text{m}$ , and a binominal least-squares fit was made\*. Using the three coefficients generated, the wavelength (or wave number) could be calculated from the drum number (n) with an accuracy of better than 0.03  $\text{cm}^{-1}$  using  $\lambda = C_1 + C_2n + C_3n^2$  with  $C_1 = 0.35746 \mu\text{m}$ ,  $C_2 = 0.9924278 \times 10^{-4} \mu\text{m}/\text{count}$ , and  $C_3 = -0.962425 \times 10^{-10} \mu\text{m}/\text{count}^2$ . It is apparent that for this particular grating and spectrometer drive gears, the scan is very nearly one angstrom per drum number (count). The spectrometer drive mechanism is also a sine bar which provides a nearly linear scan in wavelength. A precisely linear drive would leave  $C_3$  equal to zero. The system described here has a nonzero value of  $C_3$  and indicates a 1-percent correction term.

\*CO<sub>2</sub> lines from 2.68 to 2.79  $\mu\text{m}$  were also recorded but were not used.

**Table 1. Observed and Calculated Wave Numbers of the Rotation Lines  
in the (0-1) and (0-2) Bands of HF**

Spectral Line	(0-1) Band			(0-2) Band		
	Observed (cm <sup>-1</sup> )	Calculated (cm <sup>-1</sup> )	Observed Minus Calculated, (cm <sup>-1</sup> )	Observed (cm <sup>-1</sup> )	Calculated (cm <sup>-1</sup> )	Observed Minus Calculated, (cm <sup>-1</sup> )
R(10)	4301.45	4301.45	0.00	---	---	---
R(9)	4279.94	4279.94	0.00	---	---	---
R(8)	4256.33	4256.34	-0.01	7978.37	7978.37	0.00
R(7)	4230.78	4230.77	+0.01	7966.23	7966.21	+0.02
R(6)	4303.31	4203.30	+0.01	7950.70	7950.69	+0.01
R(5)	4173.99	4173.98	+0.01	7931.82	7931.84	-0.02
R(4)	4142.85	4142.85	0.00	7909.67	7909.69	-0.02
R(3)	4109.95	4109.95	0.00	7884.28	7884.28	0.00
R(2)	4075.29	4075.31	-0.02	7855.65	7855.65	0.00
R(1)	4038.96	4038.98	-0.02	7823.84	7823.84	0.00
R(0)	4001.02	4001.00	+0.02	7788.90	7788.88	+0.02
P(1)	3920.33	3920.32	+0.01	7709.73	7709.73	0.00
P(2)	3877.72	3877.71	+0.01	7665.64	7665.62	+0.02
P(3)	3833.68	3833.67	+0.01	7618.55	7618.57	-0.02
P(4)	3788.21	3788.24	-0.03	7568.62	7568.62	0.00
P(5)	3741.48	3741.47	+0.01	7517.85	7515.85	0.00
P(6)	3693.42	3693.41	+0.01	7460.30	7460.30	0.00
P(7)	3644.09	3644.11	-0.02	7402.05	7402.06	-0.01
P(8)	3593.67	3593.65	+0.02	7341.22	7341.20	+0.02
P(9)	3542.13	3542.14	-0.01	---	---	---
P(10)	3489.76	3489.75	+0.01	---	---	---

The entire spectrometer (excluding fore and exit optics) is encased in an insulated wooden box whose internal temperature is regulated to a fraction of a degree Centigrade using thermometrically controlled heating elements and air circulators. Additionally, the room in which the spectrometer is located is regulated with a continuous flow air conditioner. Despite these precautions, the calibration constant  $C_1$  or wavelength intercept varies slightly from day to day, presumably because of thermal effects.

The instrument function is also easily determined using the HF lines at  $2.7 \mu\text{m}$ . If a small amount (a few torr) of HF gas is introduced into the absorption cell, pressure broadening is negligible and Doppler broadening dominates the HF spectral lines. The spectral width of these Doppler broadened HF lines is easily calculated\* and found to be  $0.005 \text{ cm}^{-1}$  (half-width at half-height). Since this is much less than the instrument resolution, a spectral scan of a single HF absorption line will yield the spectrometer instrument function. This function closely equals a Gaussian profile, deviating only slightly in the wing region.

The resolution for the 1.83-m spectrometer was measured at  $100\text{-}\mu\text{m}$  and  $50\text{-}\mu\text{m}$  slit width settings (entrance and exit slits equal) using the P-branch lines of HF at  $2.7 \mu\text{m}$ . The resolution was found to be  $0.09$  and  $0.07 \text{ cm}^{-1}$ , respectively. The finer resolution had a signal which was a factor of four weaker, but since the signal-to-noise ratio was still about 200, this setting was used throughout the measurement program.

## 4.0 RESULTS

### 4.1 ABSORPTANCE SPECTRA

The raw data which were recorded on magnetic tape cassettes by ERIM in 1978 were read into the disk storage of the University of Michigan Amdahl 470 V/8 computer (plug compatible with the IBM 360 and 370). These data, together with the three calibration constants, allowed generation of absorptance values as a function of wave number using ERIM program JA/V10. Data output files were produced, as were computer generated (CALCOMP) spectral plots. Program JA/V10 contains an interactive plotting routine which allows manipulation of the data as dictated by wave number calibration markers, or background and zero-scan information. Since the scope of this program was to assess the utility of the measured data to update the AFGL tabulation (Ref. 1) without actually doing

---


$$^* \Delta\nu_D = \frac{v_0}{c} \left[ (\ln 2) \frac{2kT}{M} N_0 \right]^{1/2}$$

M: Molecular weight

$N_0$ : Avogadro's number

so, convenient rather than optimum accuracy was sought. As such, the wave number determination was based upon the P(J) lines of HF used to calibrate the spectrometer for the DARPA program in work performed by Peterson and Doak at ERIM. The accuracy is estimated to be on the order of  $0.1 \text{ cm}^{-1}$  with improvement to about  $0.02 \text{ cm}^{-1}$  likely with some effort based upon the markers used in the previous program (not included in the tape) and the R-branch lines of HF entailed in the  $\text{H}_2\text{O}$  spectra at 1,002K.

Since the wave number coverage for the  $2.5\text{-}\mu\text{m}$  wing was  $3,930$  to  $4,235 \text{ cm}^{-1}$  (data from  $4,235$  to  $4,300 \text{ cm}^{-1}$  were available but contained no significant spectra and were not reduced), and since single lines were roughly  $0.3 \text{ cm}^{-1}$  wide (FWHH), the data were broken into ten  $35\text{-cm}^{-1}$  regions with  $5\text{-cm}^{-1}$  overlap as shown in Table 2. The resulting spectra appear in Appendix A. Included with the experimental spectra are predicted absorption lines based upon the 1978 AFGL tabulations (Ref. 1) and adjusted for the conditions of temperature, pressure, and path length of the measurements. Figure 5 is a selected spectrum from Appendix A (see Figs. A-9 and A-10) showing the measured spectrum at the top, and the predicted spectrum (triangles — sometimes overlapping) at the bottom. These measurements were for pure water vapor and are therefore self-broadened, whereas the AFGL tabulation, used primarily for predicting atmospheric transmission, assumes foreign gas broadening (most notably  $\text{N}_2$  broadening). As such, the former are broader than the latter. The full-width-at-half-height of the measured lines is about  $0.3 \text{ cm}^{-1}$ , appreciably larger than the  $0.1 \text{ cm}^{-1}$  width of the instrument function.

**Table 2. ERIM  $2.5\text{-}\mu\text{m}$  Water Vapor Data**

	<u>Spectral Region</u>	<u>T = 1,002K</u>	<u>T = 704K</u>
		<u>P = 0.545 atm</u>	<u>P = 0.369 atm</u>
A	3,930 – 3,965 $\text{cm}^{-1}$	x	x
B	3,960 – 3,995	x	x
C	3,990 – 4,025	x	x
D	4,020 – 4,055	x	x
E	4,050 – 4,085	x	x
F	4,080 – 4,115	x	x
G	4,110 – 4,145	x	x
H	4,140 – 4,175	x	x
I	4,170 – 4,205	x	x
J	4,200 – 4,235	x	x

15-cm cell containing pure  $\text{H}_2\text{O}$   
 $0.10\text{-cm}^{-1}$  resolution

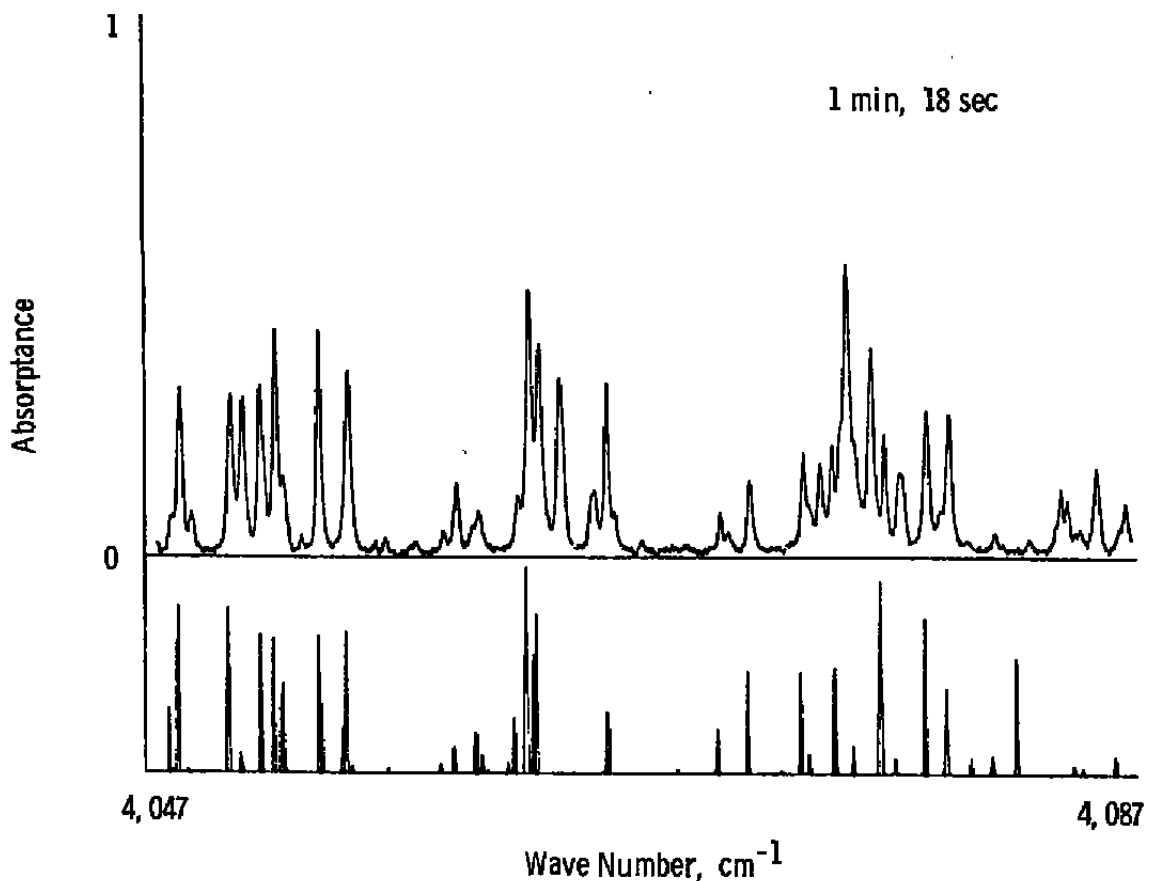


**Figure 5. Measured absorbance spectra appear at the top and corresponding computer-generated spectra appear at the bottom.**

A comparison of the observed and predicted spectra in Fig. 5 shows good agreement with respect to spectral line positions. Line intensities (area under the absorbance spectral line or triangle), however, show generally poor agreement.

#### **4.2 LINE PARAMETERS DETERMINATION**

The transmission,  $\tau$ , of optical radiation in the presence of an absorbing molecular specie follows Beer's law or

$$\tau = e^{-ku} \quad (1)$$



where  $k$  is the absorption coefficient and  $u$  is the optical path length. Since optical path length ( $u$ ) depends upon the physical length ( $L$ ) of the path and upon the quantity of absorber,  $u$  is often expressed in molecules/cm<sup>2</sup> [or atmosphere  $\times$  cm, normalized to standard temperature (273K) and pressure (760 torr)]. The absorption coefficient therefore has units of cm<sup>2</sup>/molecules (or atm<sup>-1</sup> cm<sup>-1</sup>) and depends upon wavelength or frequency, i.e.,  $k(\nu)$ . For a low-pressure gas,  $k(\nu)$  follows a Doppler distribution. For high gas pressures (greater than 100 torr for H<sub>2</sub>O), the distribution is Lorentzian in shape and the line pressure is termed broadened. Its frequency distribution is

$$k(\nu) = \frac{S \alpha / \pi}{(\nu - \nu_0)^2 + \alpha^2} \quad (2)$$

where  $\nu_0$  is the line center,  $\alpha$  is the half-width at half-height of the line, and  $S$  is the line strength for the transition.

The line strength, or line intensity ( $S$ ), is temperature ( $T$ ) dependent through the Boltzmann factor, and the rotational ( $Q_r$ ) and vibrational ( $Q_v$ ) partition functions as

$$S(T) = S(T_s) \frac{Q_v(T_s)}{Q_v(T)} \frac{Q_r(T_s)}{Q_r(T)} \exp \left[ \frac{E}{\alpha} \left( \frac{1}{T_s} - \frac{1}{T} \right) \right] \quad (3)$$

where  $T_s$  is taken to be 296K (although standard temperature is often taken as 273K),  $\alpha$  is the Boltzmann constant  $1.38 \times 10^{-23}$  joule  $^{\circ}\text{K}^{-1}$ , and  $E$  is the energy in joules for the lower state involved in the transition. Since the vibrational partition function increases only slightly with increasing temperature, and the rotational partition function is proportional to  $T^m$  where  $m = 3/2$  for H<sub>2</sub>O, Eq. (3) may be rewritten as

$$S(T) = S(T_s) \left( \frac{T_s}{T} \right)^{3/2} \exp \left[ 1.439 E'' \left( \frac{1}{T_s} - \frac{1}{T} \right) \right] \quad (4)$$

or

$$S(T_s) = S(T) \left( \frac{T}{T_s} \right)^{3/2} \exp \left[ 1.439 E'' \left( \frac{1}{T} - \frac{1}{T_s} \right) \right] \quad (5)$$

where  $E''$  is the lower state energy, now expressed in  $\text{cm}^{-1}$ . Measurement of  $S$  at two or more temperatures allows determination of  $E''$  and, knowing  $E''$  and  $S$  at a single temperature allows computation of  $S$  at any other temperature.

Since the work statement of this program called for a cursory (one man-week of effort) determination of line strengths, widths, and lower state energies for a selected number of absorption lines, spectral region E was examined from 4,050 to 4,085  $\text{cm}^{-1}$ . Numerous lines appear in this region but are not heavily overlapped.

Since the parameters determination was restricted, certain approximations were made in the analysis. It was first assumed that a particular line, although convolved with the instrument function (Gaussian), follows a Lorentzian distribution with frequency. This is reasonable since the full-width at half-height of a measured line is about 0.3  $\text{cm}^{-1}$  and the instrument width is about 0.1  $\text{cm}^{-1}$ . Assuming that the widths sum as their squares, it is concluded that the true width is about 0.283  $\text{cm}^{-1}$ , only 6 percent less than the measured 0.3  $\text{cm}^{-1}$ .

Combining Eqs. (1) and (2) produces an expression for the absorptance ( $A$ ) as a function of frequency

$$A(\nu) = 1 - \tau(\nu) = 1 - \exp \left[ - \frac{Su \alpha / \pi}{(\nu - \nu_0)^2 + \alpha^2} \right] \quad (6)$$

The absorption at the peak ( $\hat{A}$ ) is therefore

$$\hat{A} = A(\nu_0) = 1 - \exp \left[ - \frac{Su}{\alpha \pi} \right]$$

Thus, if the peak absorptance, spectral width (HWHH), and optical path length (molecules/ $\text{cm}^2$ ) are taken from measurements at temperature  $T$ , the line strength at temperature  $T$  can be determined as

$$S(T) = -\pi \alpha \frac{\ln(1 - \hat{A})}{u} \quad (7)$$

The lower state energy  $E''$  could have been determined from the  $S(1,000\text{K})$  and  $S(700\text{K})$  computations. However, it was decided to determine  $E''$  directly from  $\hat{A}(1,000\text{K})$  and  $\hat{A}(700\text{K})$ , thereby eliminating error associated with the measurement of  $\alpha$ . To do so, it was assumed that water vapor is resonantly self-broadened and as such,  $\alpha$  is proportional to

pressure and inversely proportional to temperature\* (nonresonant or foreign gas broadening is inversely proportional to the square root of temperature), that is

$$\frac{\alpha(T_2)}{\alpha(T_1)} = \frac{P(T_2)}{P(T_1)} \frac{T_1}{T_2} \quad (8)$$

Solving Eqs. (4) and (5) for  $E''$  gives

$$E'' = 0.6949 \left( \frac{1}{T_1} - \frac{1}{T_2} \right)^{-1} \ell_n \left[ \frac{S(T_2)}{S(T_1)} \left( \frac{T_1}{T_2} \right)^{3/2} \right] \quad (10)$$

Using Eqs. (7) and (8) gives

$$E'' = 0.6949 \left( \frac{1}{T_1} - \frac{1}{T_2} \right)^{-1} \ell_n \left[ \frac{\ell_n(1-A_2)}{\ell_n(1-A_1)} \frac{\alpha(T_2)}{\alpha(T_1)} \right]$$

Since the optical path length is

$$u = L p \frac{273}{T} N_0$$

where  $L$  is the physical path length in cm,  $p$  is the pressure in atmospheres,  $T$  is the absolute temperature, and  $N_0$  is the number of molecules per  $\text{cm}^3$  at standard temperature (273K) and pressure ( $2.69 \times 10^{19}$  molecules/ $\text{cm}^3$  for an ideal gas), Eqs. (7) and (8) may be used to rewrite Eq. (10) as

$$\begin{aligned} E'' &= 0.6949 \left( \frac{1}{T_1} - \frac{1}{T_2} \right)^{-1} \ell_n \left[ \frac{\ell_n(1-\hat{A}_2)}{\ell_n(1-\hat{A}_1)} \frac{\alpha(T_2)}{\alpha(T_1)} \frac{u(T_1)}{u(T_2)} \left( \frac{T_2}{T_1} \right)^{3/2} \right] \\ &= 0.6949 \left( \frac{1}{T_1} - \frac{1}{T_2} \right)^{-1} \ell_n \left[ \frac{\ell_n(1-A_2)}{\ell_n(1-A_1)} \left( \frac{T_2}{T_1} \right)^{3/2} \right] \end{aligned} \quad (11)$$

\*More precisely,

$$\alpha(P,T) = \gamma_{\text{res}} p \frac{273}{T} + \gamma_{\text{non-res}} p \sqrt{\frac{273}{T}} \quad (9)$$

where  $\gamma_{\text{res}} = 0.44 \text{ cm}^{-1}/\text{atm}$   
 $\gamma_{\text{non-res}} = 0.07 \text{ cm}^{-1}/\text{atm}$

for  $\text{H}_2\text{O}$ . Neglecting the nonresonant part results in only a 4-percent difference in line width ratios for  $T_1 = 700\text{K}$  and  $T_2 = 1,000\text{K}$ .

Table 3 presents the results of hand reduced line parameters for ten absorption lines from scan E (see Figs. 5, A-9, A-10, A-29, and A-30). For each of the ten lines, line center frequency ( $\nu_0$ )\*, peak absorptance  $\hat{A}(T,P)$ , and line half-width at half-height  $\alpha(T,P)$  are tabulated as taken from experimental measurements for both 1,000K and 700K. From these values, the lower state energy ( $E''$ ) was calculated from Eq. (11) and  $S(T)$  was calculated from Eq. (7). Based upon values of  $\nu_0$ ,  $E''$ , and  $S(T)$ , the AFGL Line Parameters Compilation was examined (Table 3) for a tabulation line which provided a close match. If such a line was found (all except the 4063.79  $\text{cm}^{-1}$  line) the tabulated  $E''$  was used rather than the experimental value, since the AFGL believes that its tabulated  $E''$  values are accurate to a few  $\text{cm}^{-1}$ . Also, since most of the lines in the wing region have computed line positions, and since energy levels must be known with fair accuracy to determine line position to a factor of a wave number, it may be concluded that the tabulated lower state energy has an accuracy of at least a few wave numbers if the line can be found at all in the tabulation. The experimentally determined  $S(T_s)$  value was thus computed using the tabulated  $E''$  wherever possible and appears in Table 3. For comparison, the tabulated value of  $S(T_s)$  is presented. Here, however, because of the difficulties in calculating vibration-rotation line strengths for asymmetric top molecules such as  $\text{H}_2\text{O}$ , ERIM's strengths are believed to be significantly more accurate than the tabulated values. As stated in Ref. 1: for the low-J lines of the strongest bands, the accuracy of the line intensity should be within  $\pm 10$  percent; it should be within a factor of two for other lines of sufficient intensity ( $> 10^{-25} \text{ cm}^{-1}/\text{mol} \cdot \text{cm}^{-2}$ ) to appear in laboratory or solar spectra, and within an order of magnitude for the weakest lines.

Attention is called to two particular lines in Table 3. The first, at 4063.79  $\text{cm}^{-1}$  is not present at all in the tabulation. The second, at 4079.53  $\text{cm}^{-1}$  is a line which is strong even at room temperature and hence should be known to the stated accuracy of  $\pm 10$  percent. There is, however, a factor of two discrepancy between the computed line strength based upon ERIM measurements and the strength which appears in the tabulation. Note also that the ERIM  $E''$  value for this line is 35 percent lower than the tabulated value. The accuracy of ERIM's  $E''$  is expected to be quite low since  $S$  can be seen to vary only slightly with temperature.

---

\*A strong spectral line appears at 4075.40  $\text{cm}^{-1}$  which is not present in the AFGL tabulation. This is believed to be a remnant of the HF gas used to calibrate the 3- $\mu\text{m}$  spectral region and which is being driven out of the cell walls at the high temperature of 1,000K. The line position of 4075.40  $\text{cm}^{-1}$  is in fair agreement with the accepted value of  $4075.32 \pm 0.02 \text{ cm}^{-1}$  (Ref. 3).

**Table 3. Spectral Line Parameters**

For each spectral line, the first entry corresponds to ERIM measurements and the second, for comparison, is from the AFGL tabulation.

$T = 1,000\text{K}$ ,  $P = 0.545\text{ atm}$ ,  $T_s = 296\text{K}$ ,  $P_s = 1\text{ atm}$

$\gamma_0$ ( $\text{cm}^{-1}$ )	$E''$ ( $\text{cm}^{-1}$ )	$S(T)$ ( $\text{cm}^{-1}/\text{mol}\cdot\text{cm}^2$ )	$S(T_s)^*$ ( $\text{cm}^{-1}/\text{mol}\cdot\text{cm}^2$ )	$\alpha(T,P)$ ( $\text{cm}^{-1}$ )
4054.05	3466	$2.85 \times 10^{-21}$	$2.1 \times 10^{-25}$	0.102
4054.035	3319		$1.50 \times 10^{-25}$	
4055.24	3466	$3.12 \times 10^{-21}$	$5.1 \times 10^{-25}$	0.144
4055.140	3080		$3.43 \times 10^{-25}$	
4059.62	1699	$4.3 \times 10^{-22}$	$9.4 \times 10^{-24}$	0.127
4059.500	1875		$1.7 \times 10^{-24}$	
4062.56	2389	$4.45 \times 10^{-21}$	$4.7 \times 10^{-24}$	0.134
4062.425	2534		$4.15 \times 10^{-24}$	
4063.79	3088	$3.01 \times 10^{-21}$	$4.8 \times 10^{-25}$	0.155
---	---		---	
4065.69	2845	$1.85 \times 10^{-21}$	$8.9 \times 10^{-26}$	0.099
4065.655	3437		$2.08 \times 10^{-26}$	
4071.48	2616	$1.02 \times 10^{-21}$	$3.3 \times 10^{-25}$	0.129
4071.368	2881		$2.64 \times 10^{-25}$	
4076.38	2276	$2.76 \times 10^{-21}$	$2.1 \times 10^{-24}$	0.127
4076.74	2629		$2.50 \times 10^{-24}$	
4078.61	2496	$2.05 \times 10^{-21}$	$1.9 \times 10^{-25}$	0.136
4078.536	3245		$1.4 \times 10^{-25}$	
4079.53	508	$1.72 \times 10^{-21}$	$7.4 \times 10^{-22}$	0.120
4079.403	782		$3.57 \times 10^{-22}$	

\*Whenever possible  $S(T_s)$  is computed using ERIM-measured  $S(T)$ , and the  $E''$  is taken from the AFGL tabulation.

## 5.0 CONCLUDING REMARKS

The high-temperature water vapor absorption measurements taken by ERIM in 1978 have been reduced. The measurements were made using a 1.8-m spectrometer having a resolution of  $0.10 \text{ cm}^{-1}$  at  $4,000 \text{ cm}^{-1}$  employing a 15-cm cell at temperatures of 1,000K and 700K, and pressures of 0.545 atm and 0.369 atm, respectively. The spectral coverage for the reduced spectra was from 3,930 to  $4,235 \text{ cm}^{-1}$  [similar data at six temperatures is also available from ERIM covering the spectral region from 2,950 to  $3,750 \text{ cm}^{-1}$  (Ref. 1)]. The reduced spectra appear in Appendix A, and a computer tape of these spectra has been supplied to Sverdrup Technology, Inc.

With the aid of Fig. 6, the importance of these spectra for high-temperature water vapor emission can be seen. In the figure one sees high-temperature (1,000K) water vapor emission spanning the spectral region from 3,000 to  $4,200 \text{ cm}^{-1}$ . If cool water vapor is present between the hot emitter and cool absorber, the band center is absorbed but the wing regions pass with little attenuation. It is precisely these wing regions which are poorly represented by the AFGL tabulation (Ref. 1) and at which ERIM has directed its efforts.

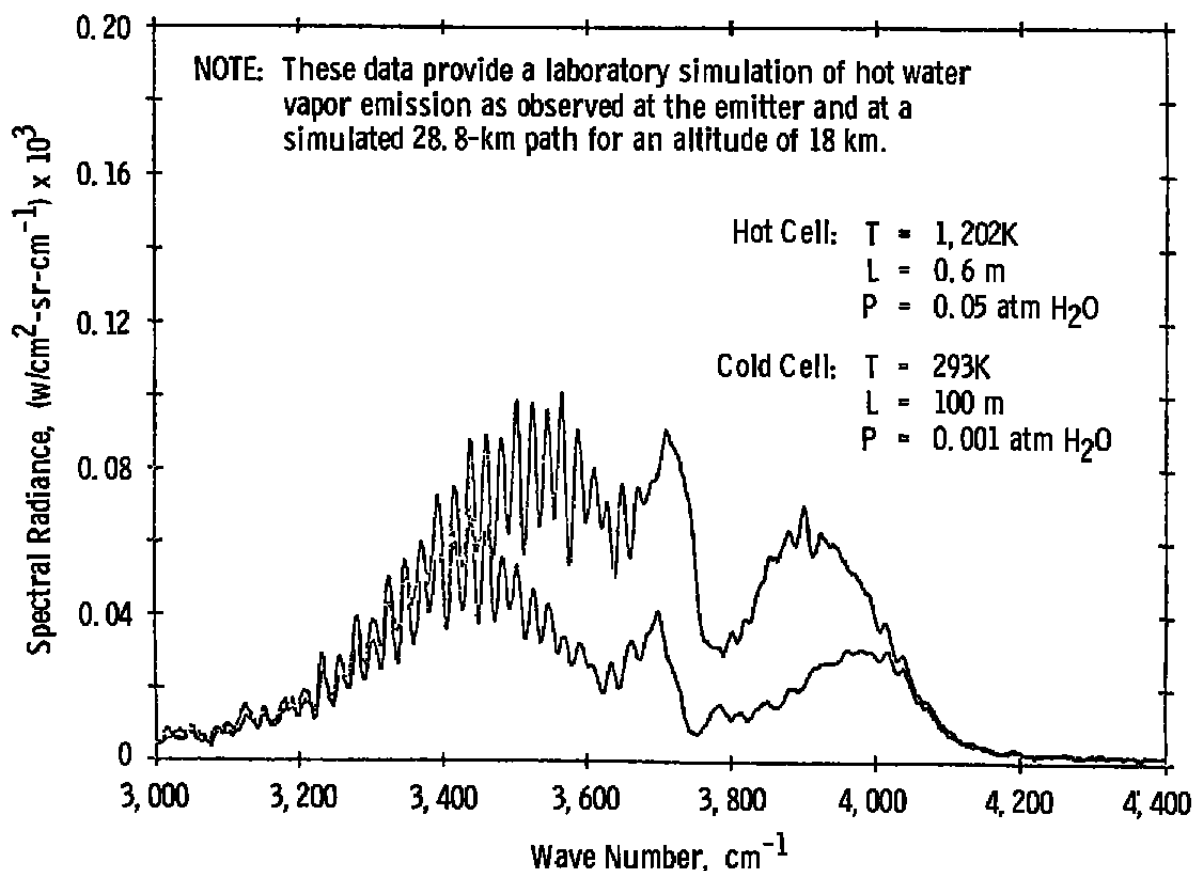


**Figure 6. Measured hot cell radiance (upper) and hot-through-cold radiance (lower).**

The scope of this particular effort allowed only a brief analysis of a few lines in a selected spectral interval. This analysis did, however, show the data to be useful in providing values of line strength, line width (self-broadened), and lower state energy, and the results appear in Table 3. Note that where line position is predicted accurately by the AFGL tabulation, the tabulated lower state energy should be relied upon over the ERIM-measured value.

It is recommended that the data be further analyzed to provide these same three parameters with improved accuracy using computer techniques, deconvolution of the instrument function from the measured spectra, and removal of overlapping lines.

It is also recommended that further measurements be undertaken to determine the effects of foreign gas broadening (most notably nitrogen) on the H<sub>2</sub>O line width, thereby completing the correction to the AFGL tabulation.

### REFERENCES

1. McClatchey, R. A. and Benedict, W. S., et al. "AFCRL Atmospheric Absorption Line Parameters Compilation." Air Force Geophysics Laboratory, AFCRL-TR-73-0096, January 1973.
2. *Handbook of Chemistry and Physics*. Chemical Rubber Publishing Co., 1963.
3. Herget, W. F. and Deeds, W. E., et al. "IR Spectrum of Hydrogen Fluoride: Line Positions and Line Shapes, Part II, Treatment of Data and Results." *Journal of the Optical Society of America*, Vol. 52, No. 10, October 1962, pp. 1113-1119.

## APPENDIX A

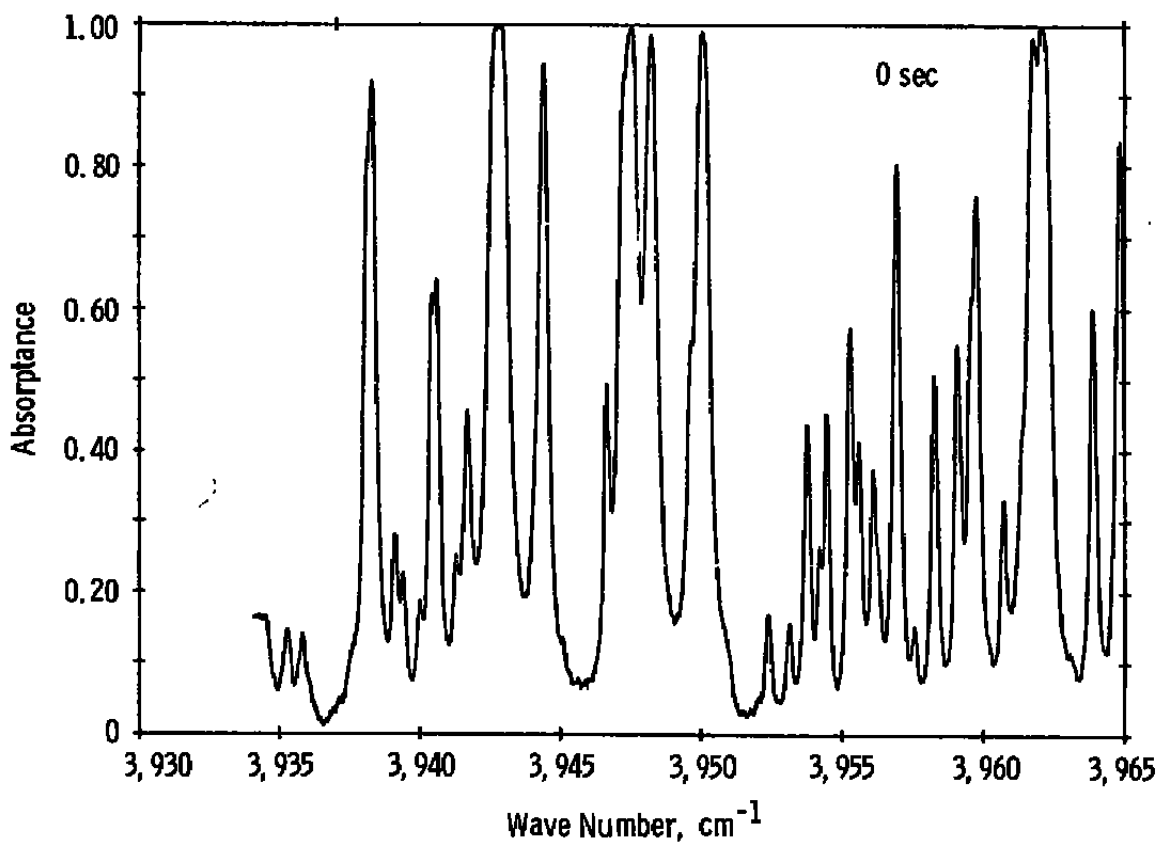
### WATER VAPOR SPECTRA FROM 3,930 TO 4,235 $\text{cm}^{-1}$

Table A-1 summarizes the experimental conditions under which the water vapor absorption measurements were made. The following figures constitute a series of spectral scans corresponding to Run H for water vapor at a temperature of 1,002K and a pressure of 414 torr (0.545 atm) and Run I at a temperature of 704K and a pressure of 280 torr (0.369 atm). The measured absorption spectra are compared to computed spectra based upon the AFGL line-by-line tabulation\*. The latter are represented by triangles whose height and width are appropriate for the experimental conditions of temperature, pressure, path length, and instrument function. The even-numbered figures provide a comparison between the observed spectra and the AFGL tabulation. The experimentally-measured spectra appear at the top, and directly below are the corresponding lines of the computer generated spectra. The odd-numbered figures are the same experimentally measured spectra but with graduated ordinate and abscissa.

---

\*A computer tape of the 1978 version of the AFGL tabulation was obtained from the National Climatic Center, NOAA, Asheville, N. C.





**Figure A-1. H<sub>2</sub> absorption in spectral range 3,930 to 3,965 cm<sup>-1</sup>, 1,002K, 414 torr.**

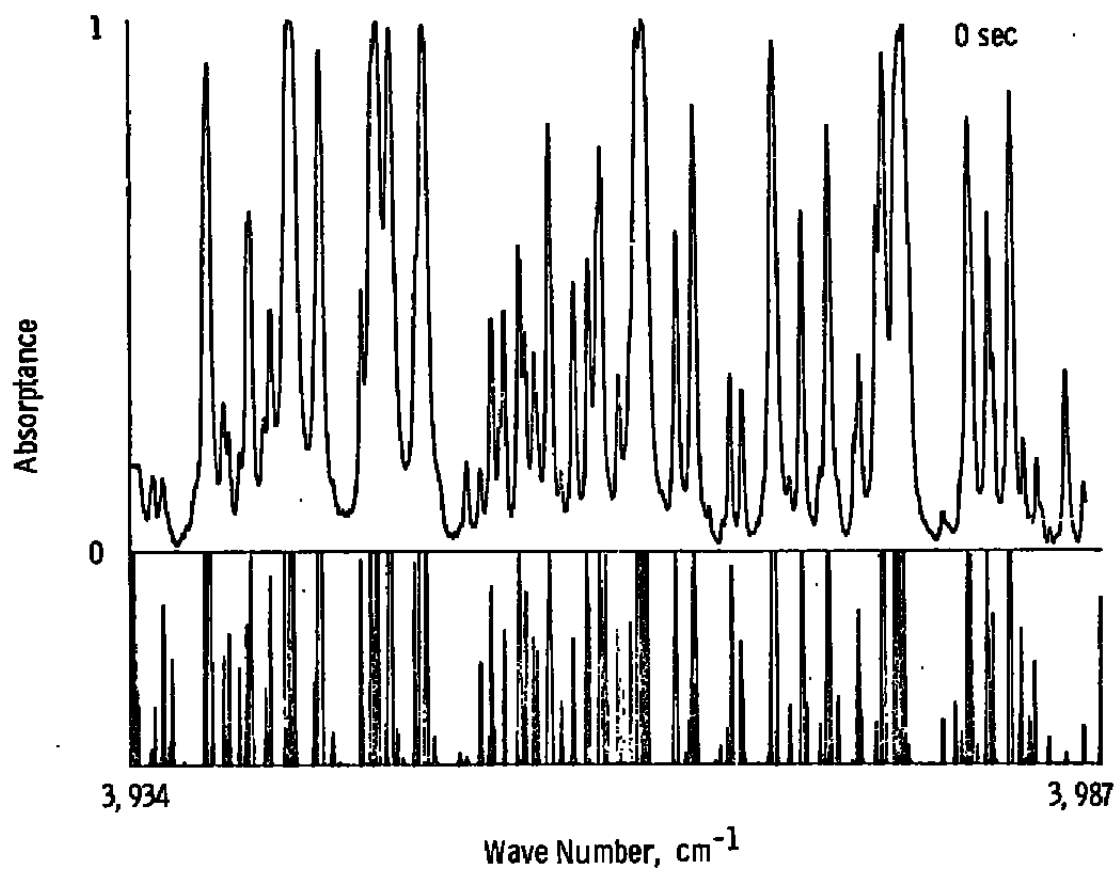


**Figure A-2. Comparison of  $\text{H}_2\text{O}$  spectrum and AFGL line atlas, 3,934 to 3,987  $\text{cm}^{-1}$ , 1,000K, 414 torr.**

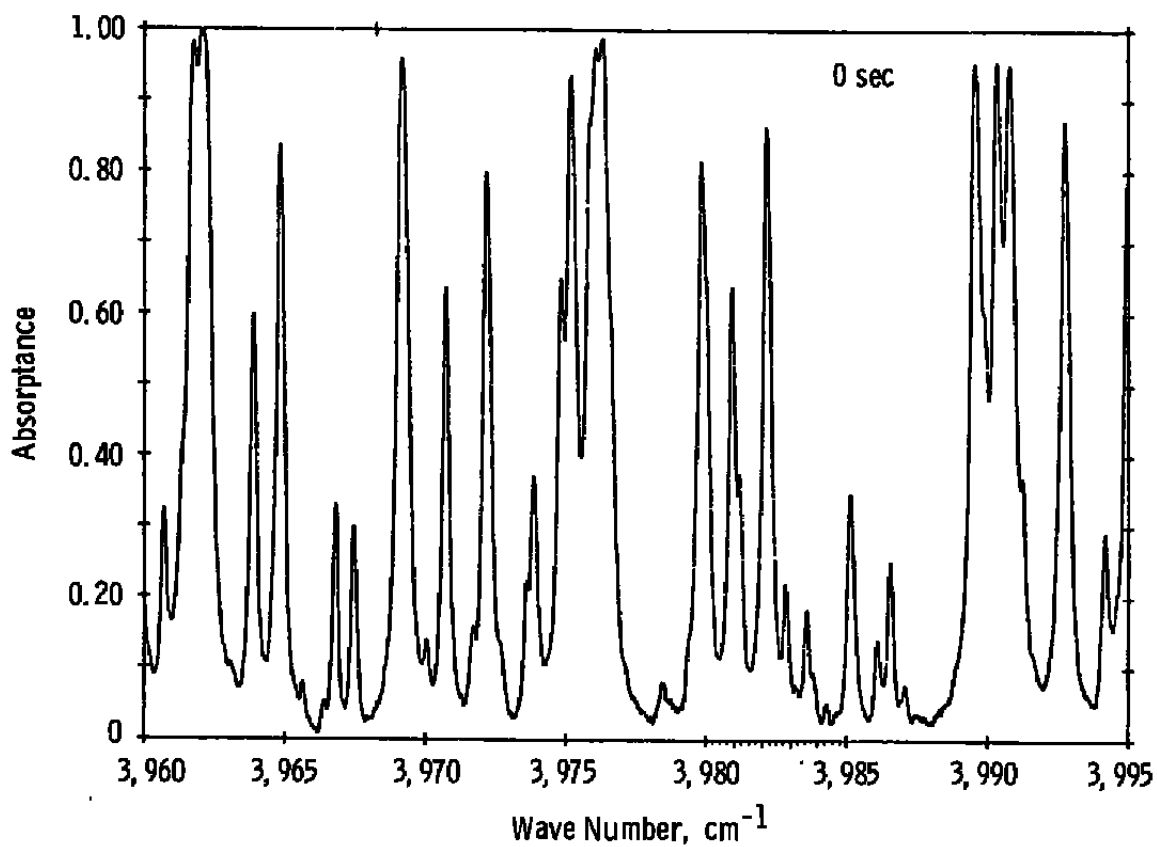


**Figure A-3. H<sub>2</sub>O absorption in spectral range 3,960 to 3,995 cm<sup>-1</sup>, 1,002K, 414 torr.**

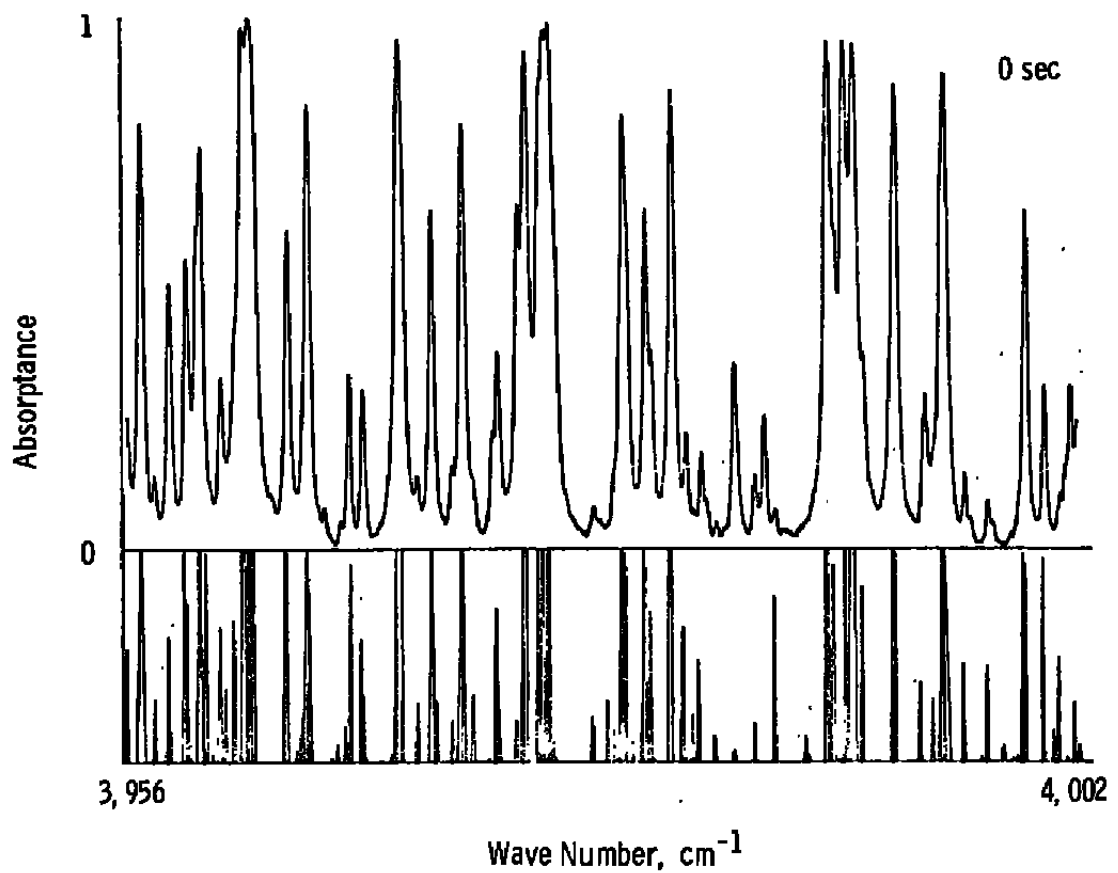


**Figure A-4. Comparison of  $\text{H}_2\text{O}$  spectrum and AFGL line atlas, 3,956 to 4,002  $\text{cm}^{-1}$ , 1,002K, 414 torr.**

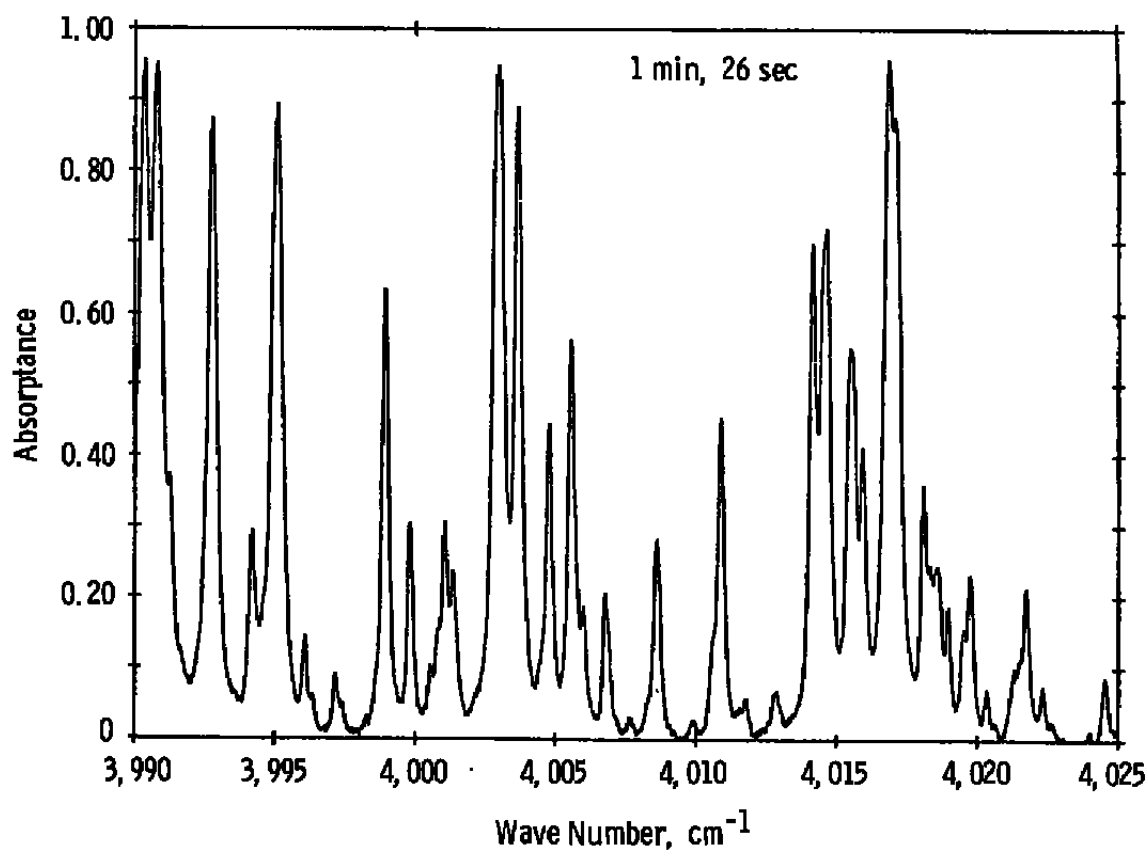
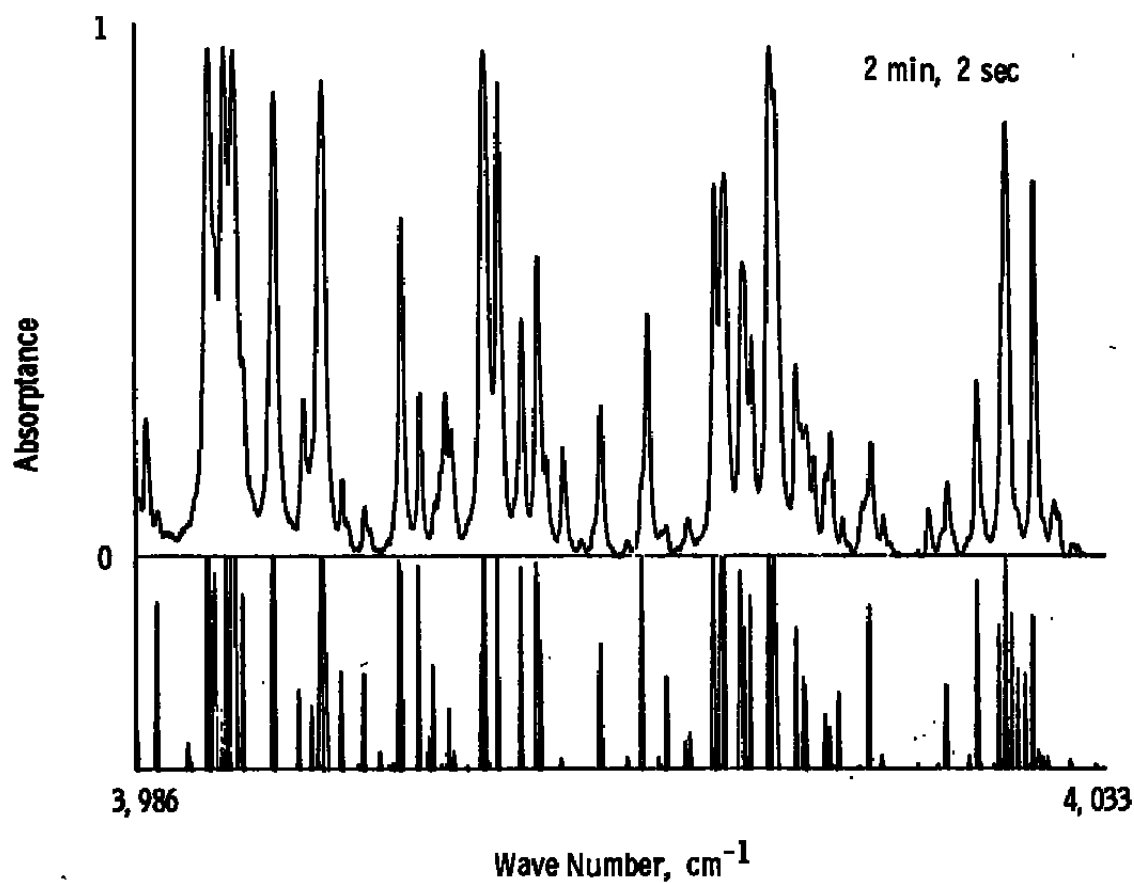


Figure A-5. H<sub>2</sub> absorption in spectral range 3,990 to 4,025 cm<sup>-1</sup>, 1,002K, 414 torr.



**Figure A-6. Comparison of  $H_2O$  spectrum and AFGL line atlas 3,986 to 4,003  $cm^{-1}$ , 1,002K, 414 torr.**

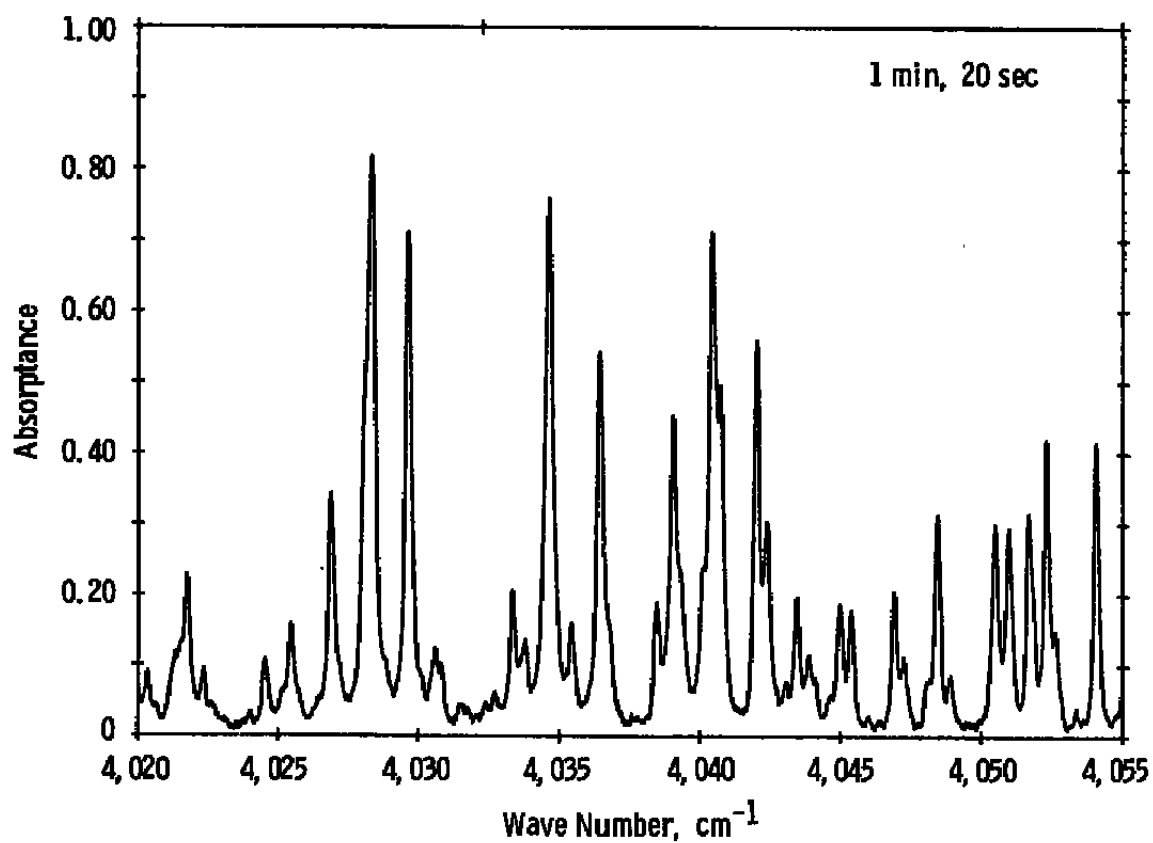


Figure A-7. H<sub>2</sub>O absorption in spectra range 4,020 to 4,055 cm<sup>-1</sup>, 1,002K, 414 torr.

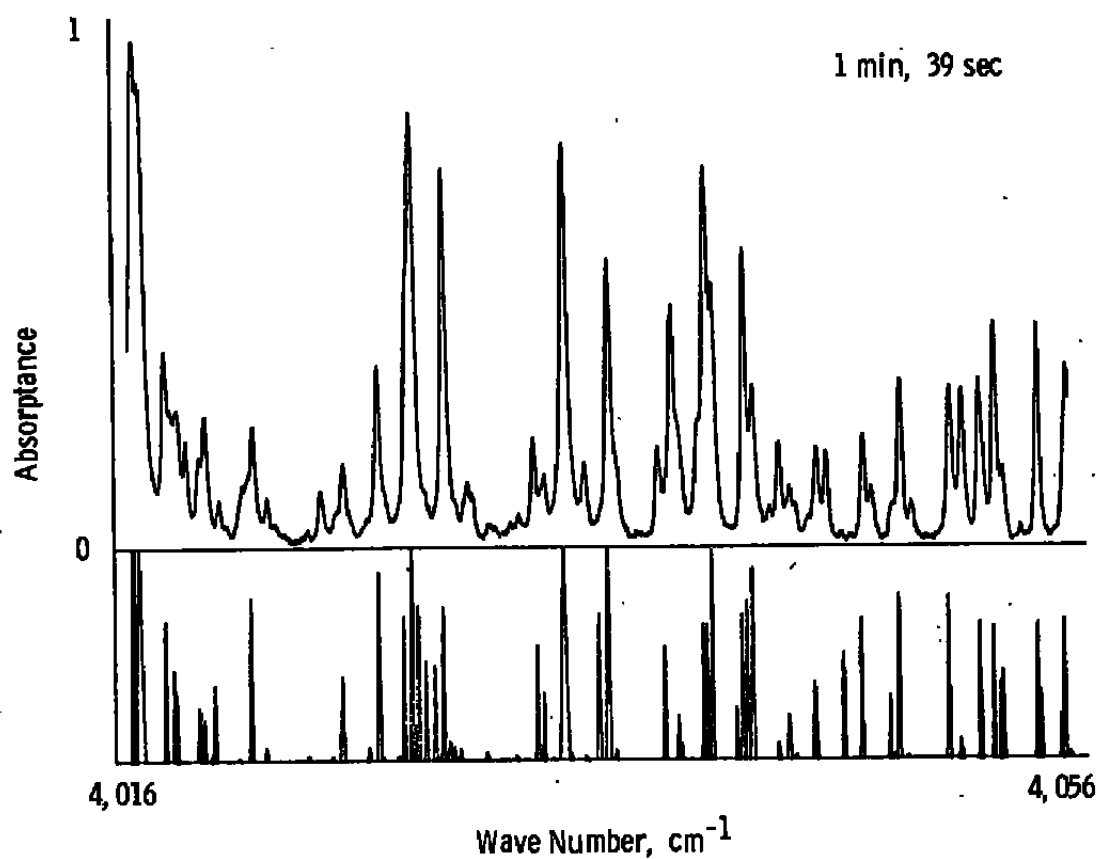


Figure A-8. Comparison of  $H_2O$  spectrum and AFGL line atlas, 4,016 to 4,056  $cm^{-1}$ , 1,002K, 414 torr.



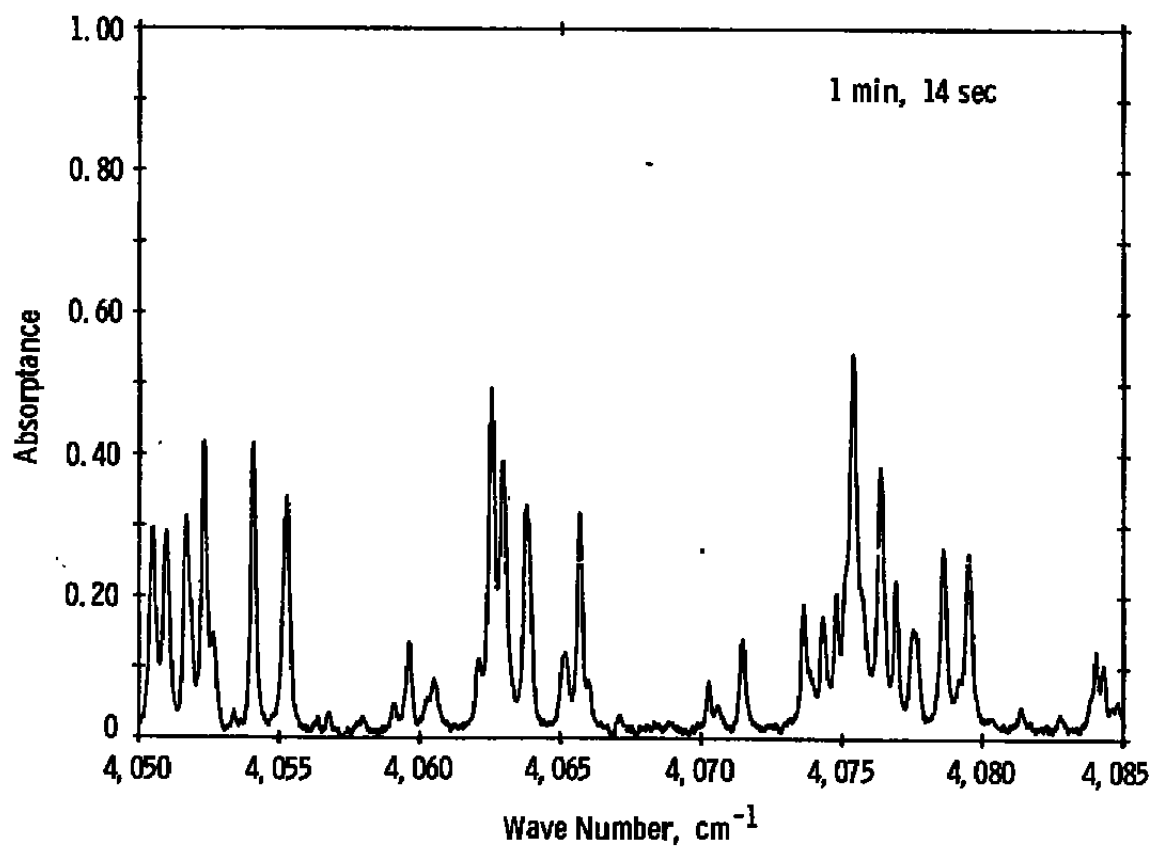
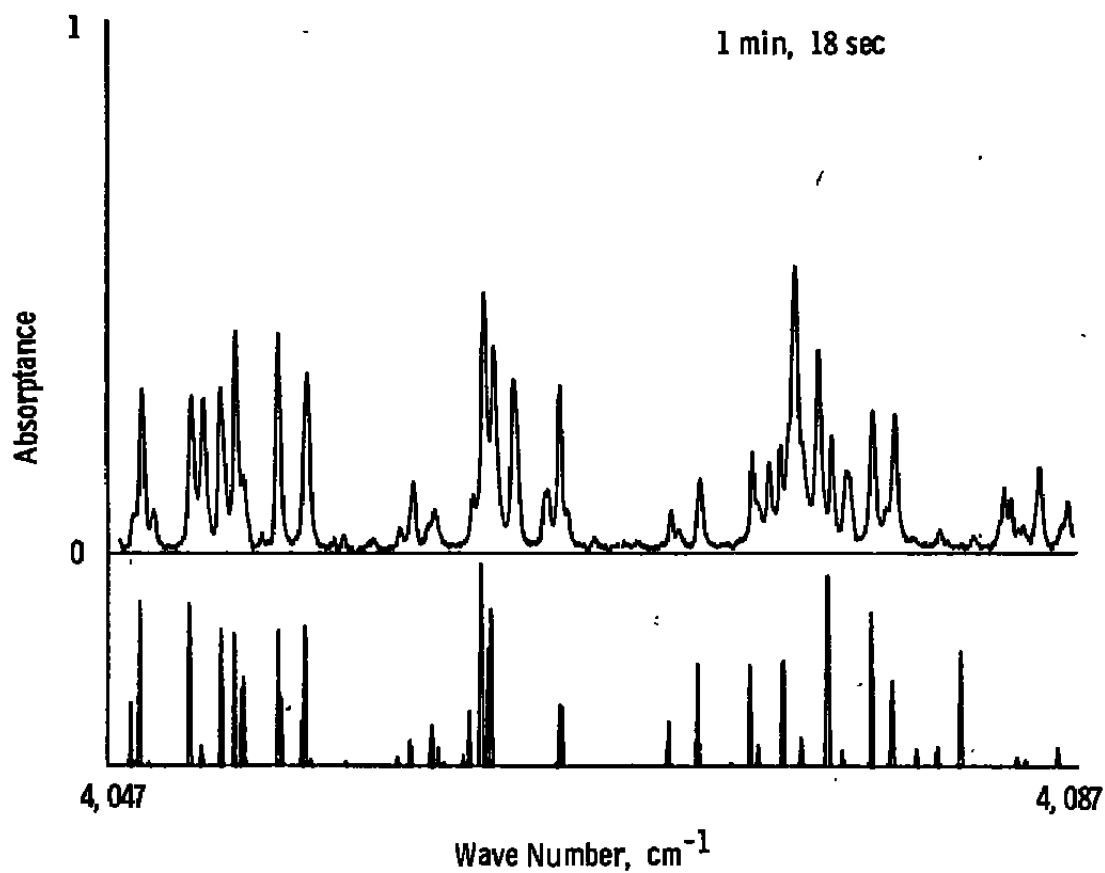
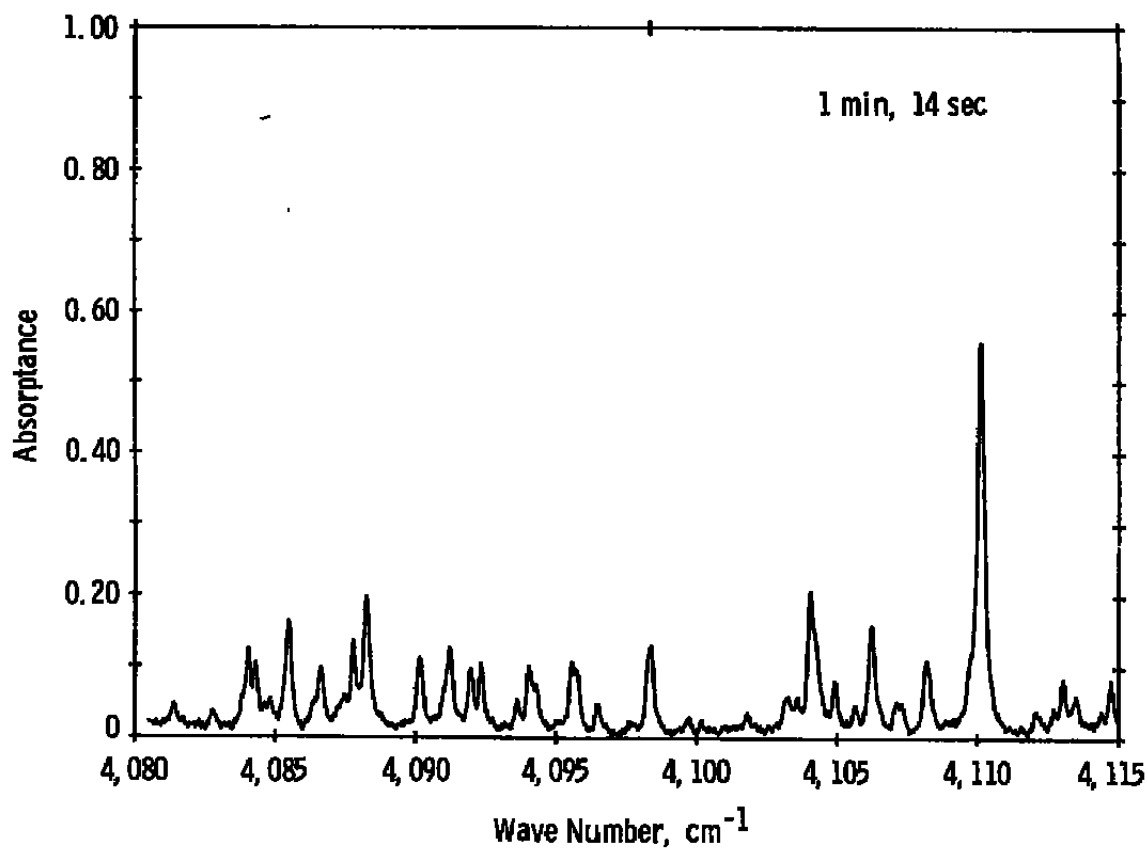


Figure A-9. H<sub>2</sub>O absorption in spectral range 4,050 to 4,085 cm<sup>-1</sup>, 1,002K, 414 torr.



**Figure A-10. Comparison of  $\text{H}_2\text{O}$  spectrum and AFGL line atlas 4,047 to 4,087  $\text{cm}^{-1}$ , 1,002K, 414 torr.**



**Figure A-11. H<sub>2</sub>O absorption in spectral range 4,080 to 4,115 cm<sup>-1</sup>, 1,002K, 414 torr.**

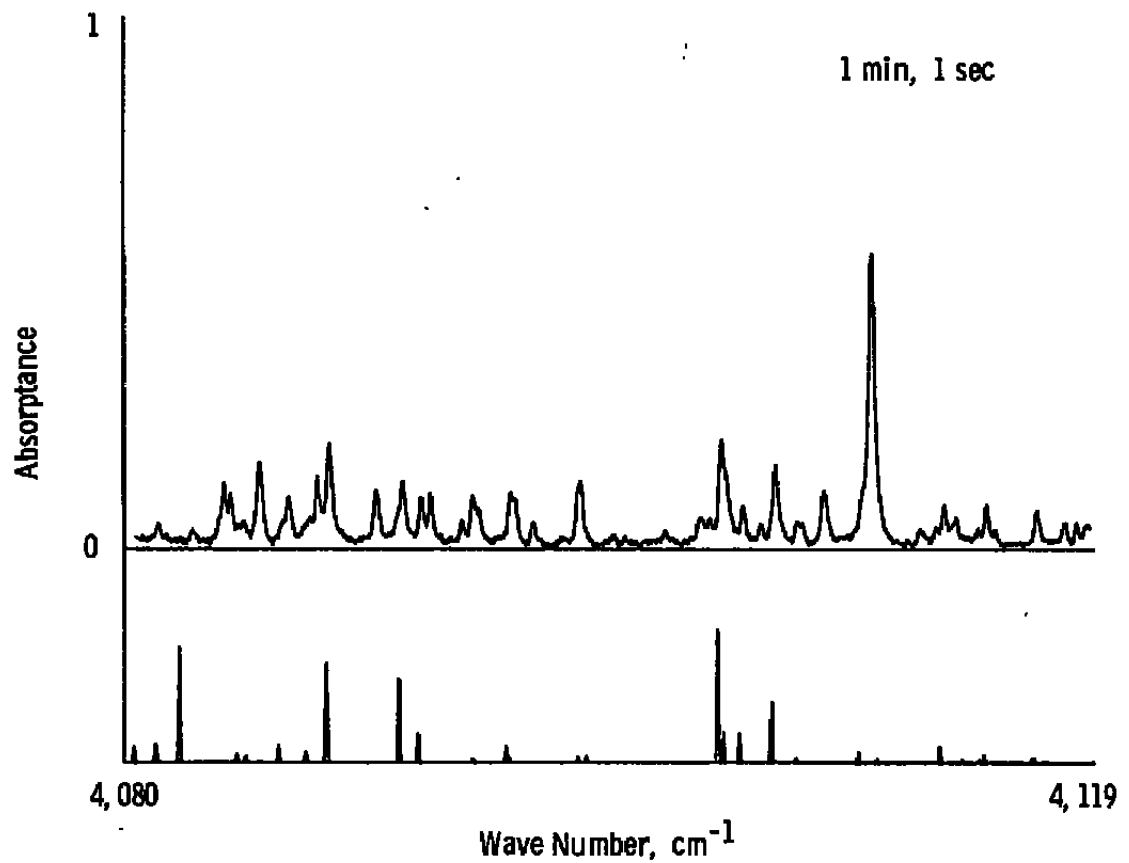


**Figure A-12. Comparison of H<sub>2</sub>O spectrum and AFGL line atlas, 4,080 to 4,119 cm<sup>-1</sup>, 1,002K, 414 torr.**

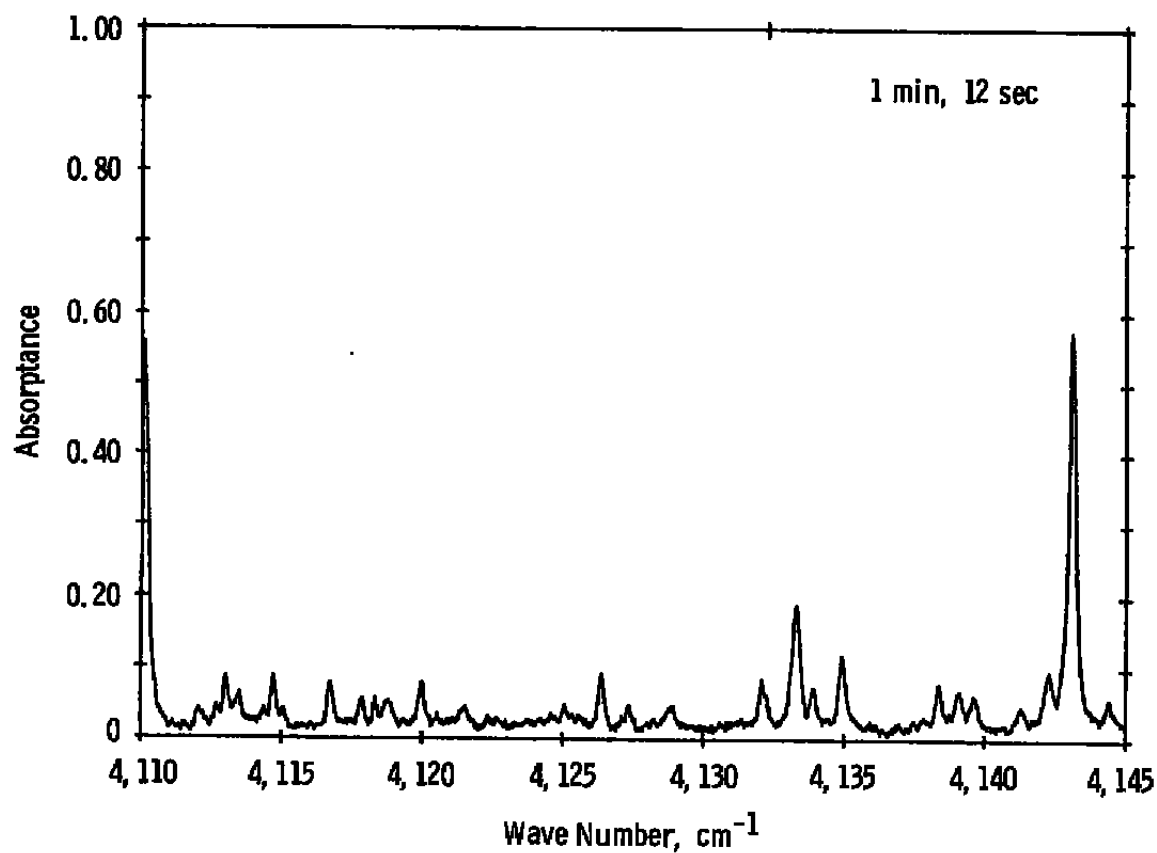


**Figure A-13. H<sub>2</sub>O absorption in spectral range 4,110 to 4,145 cm<sup>-1</sup>, 1,002K, 414 torr.**

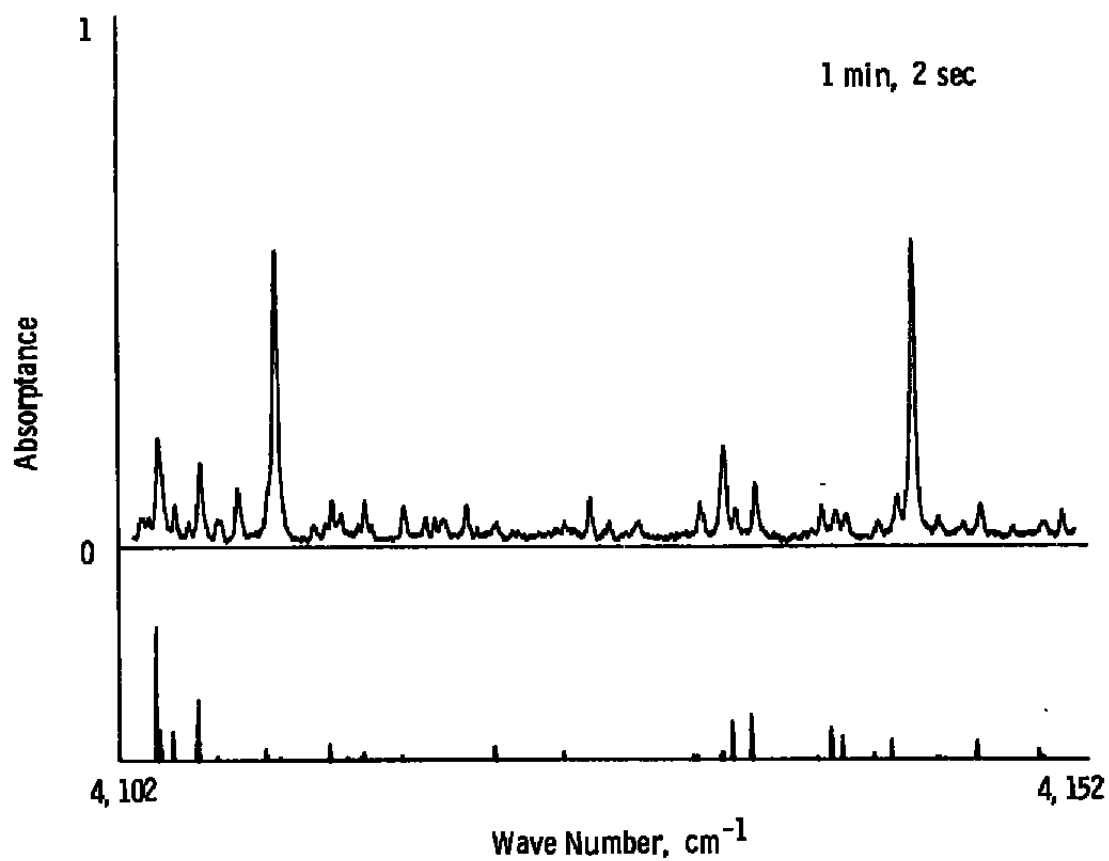
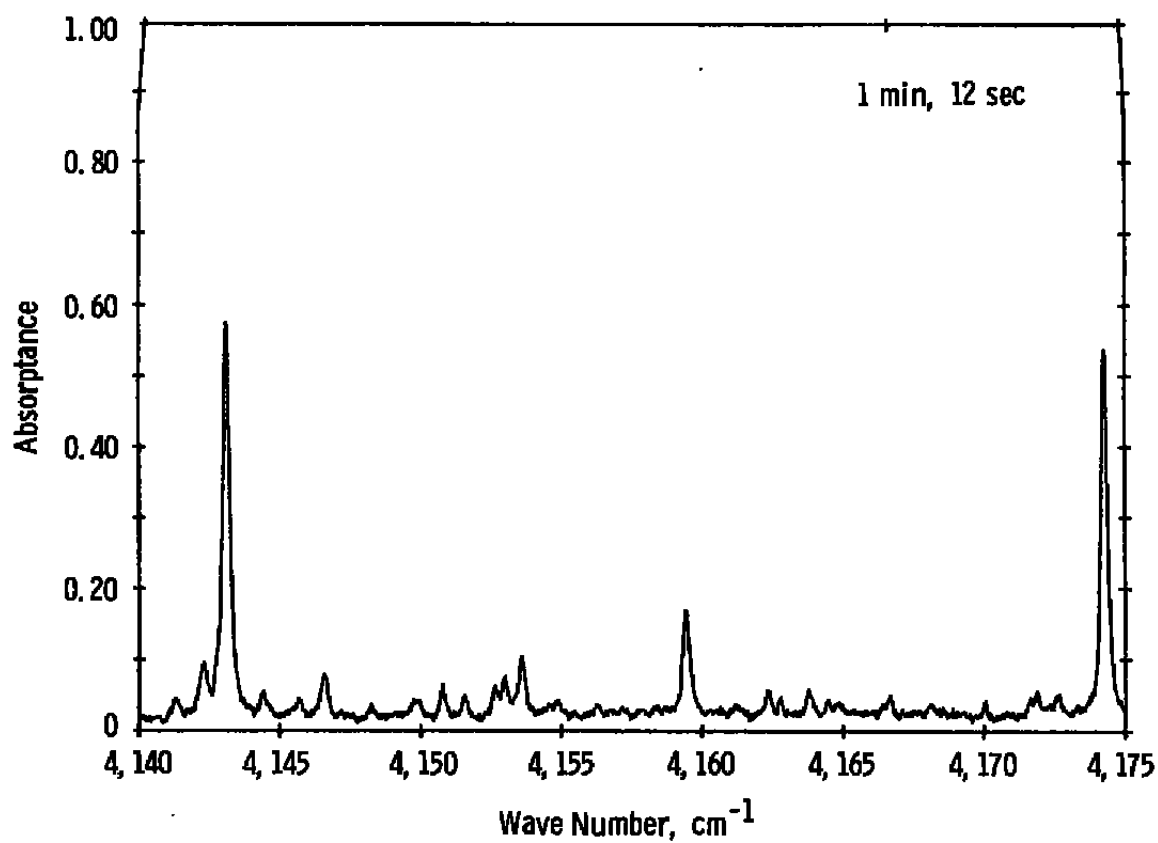
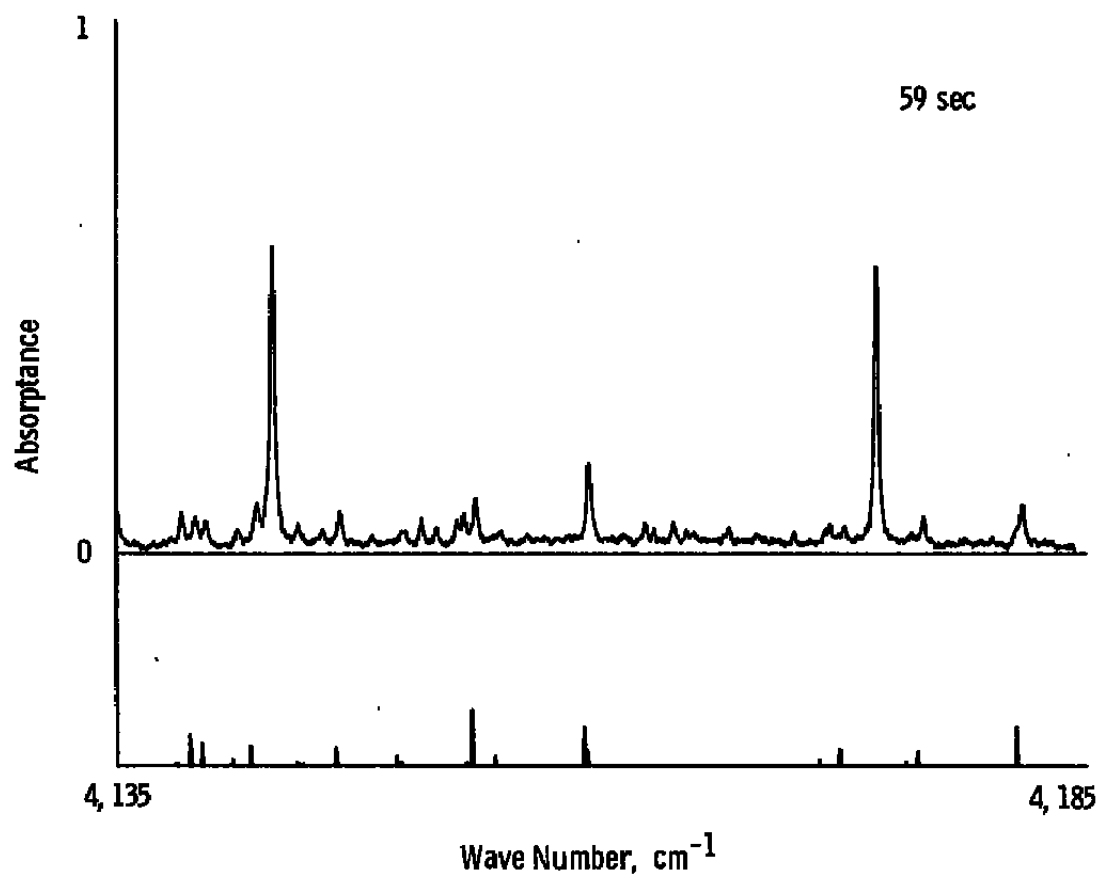


Figure A-14. Comparison of  $\text{H}_2\text{O}$  spectrum and AFGL line atlas, 4,102 to 4,152  $\text{cm}^{-1}$ , 1,002K, 414 torr,  $\circ$



**Figure A-15. H<sub>2</sub>O absorption in spectral range 4,140 to 4,175 cm<sup>-1</sup>,  
1,002K, 414 torr.**

o



**Figure A-16. Comparison of  $\text{H}_2\text{O}$  spectrum and AFGL line atlas, 4,135 to 4,185  $\text{cm}^{-1}$ , 1,002K, 414 torr.**



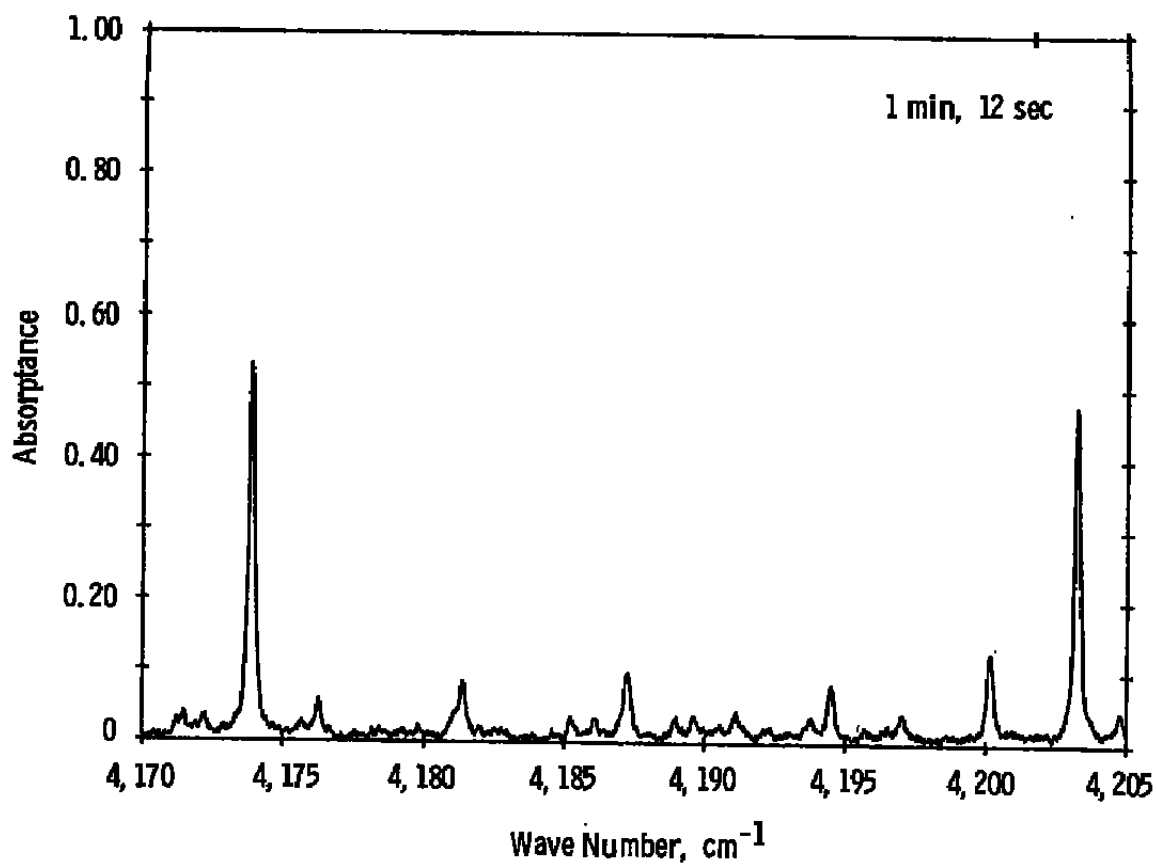


**Figure A-17. H<sub>2</sub>O absorption in spectral range 4,170 to 4,205 cm<sup>-1</sup>, 1,002K, 414 torr.**

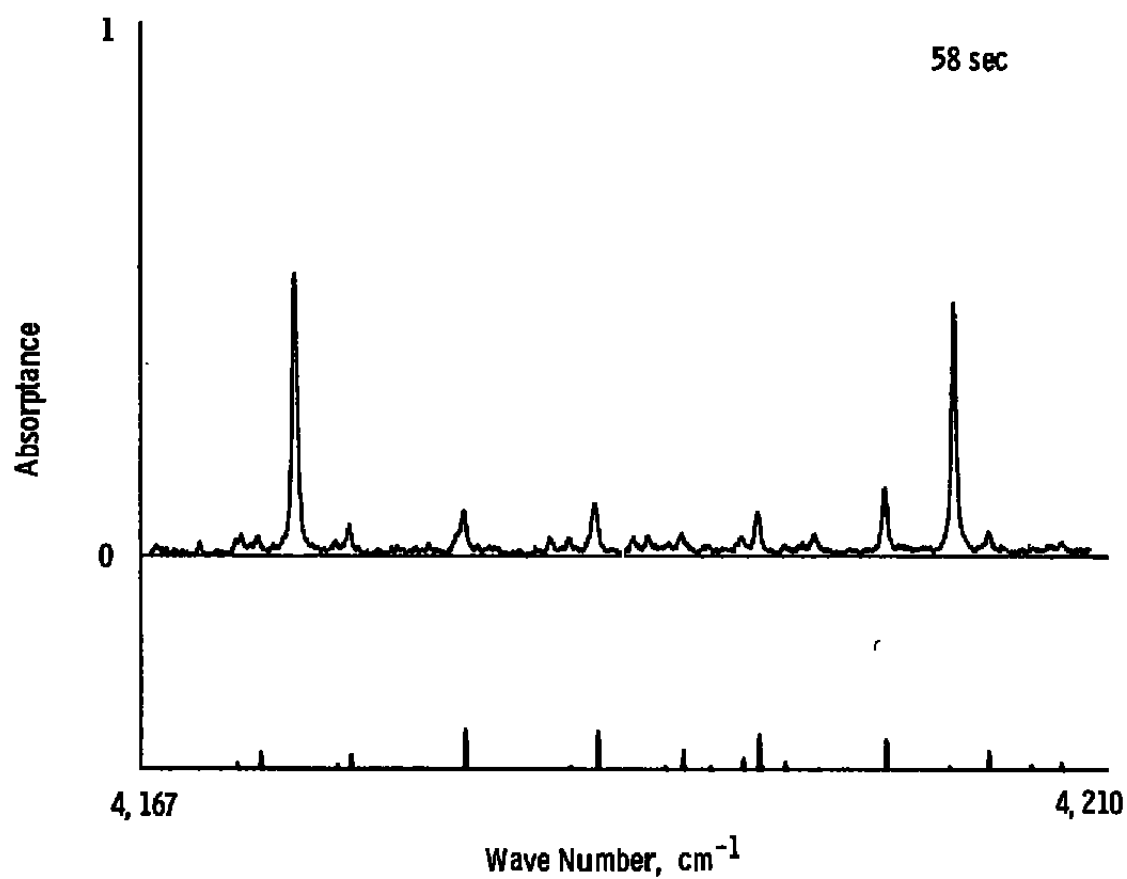


**Figure A-18. Comparison of  $\text{H}_2\text{O}$  spectrum and AFGL line atlas, 4,167 to 4,210  $\text{cm}^{-1}$ , 1,002K, 414 torr.**

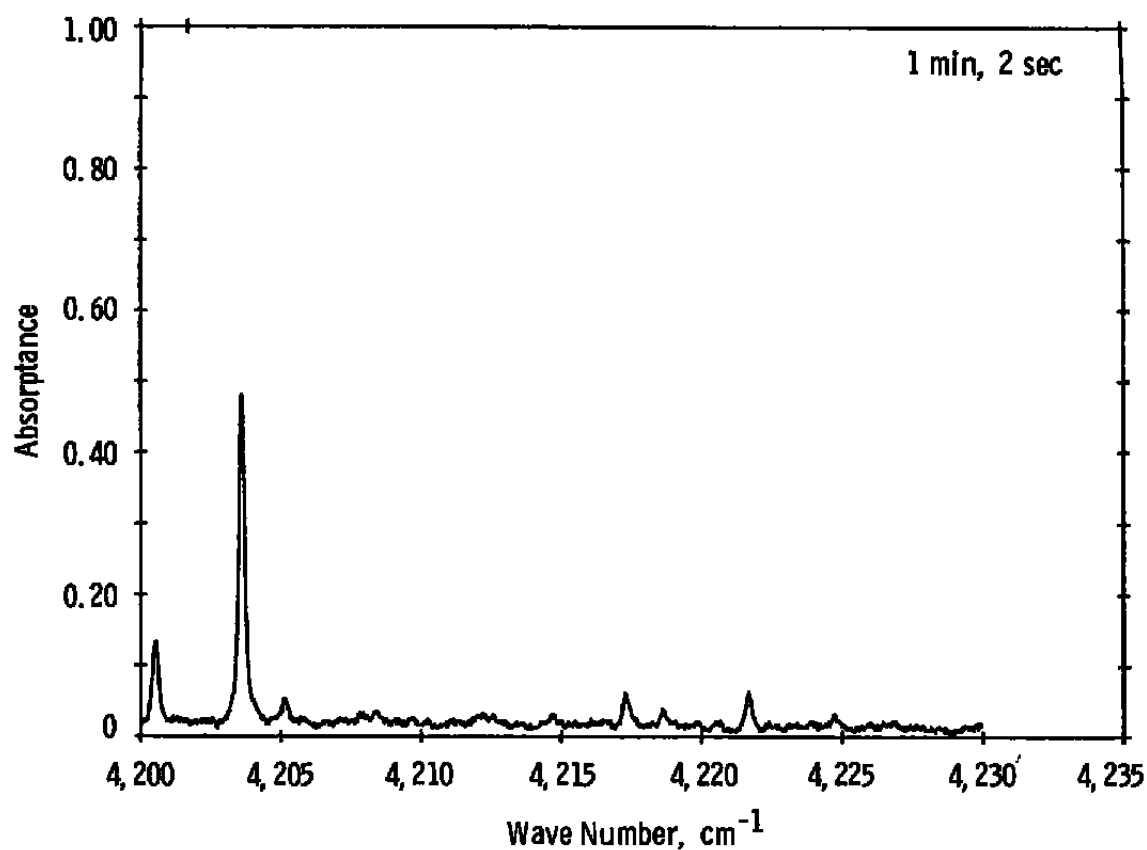


**Figure A-19. H<sub>2</sub>O absorption in spectral range 4,200 to 4,235 cm<sup>-1</sup>,  
1,002K, 414 torr.**

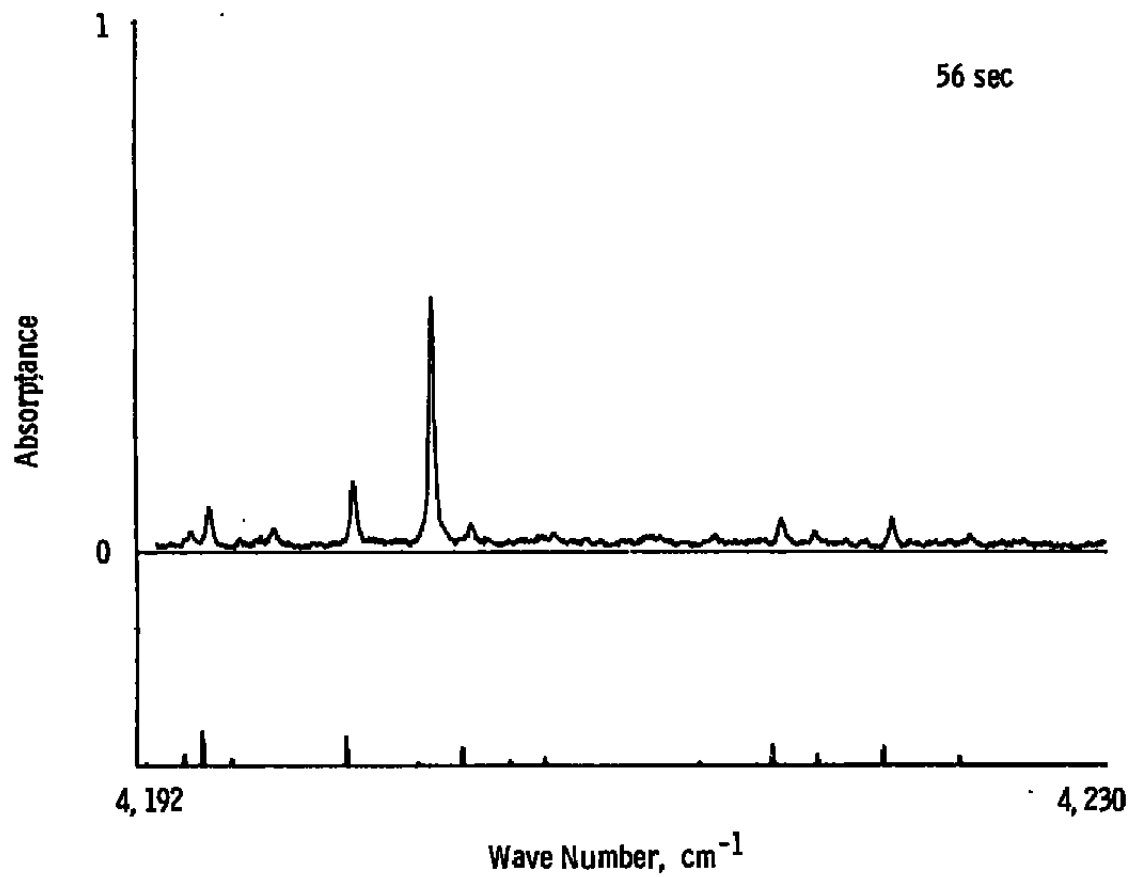


**Figure A-20. Comparison of H<sub>2</sub>O spectrum and AFGL line atlas, 4,190 to 4,230 cm<sup>-1</sup>, 1,002K, 414 torr.**

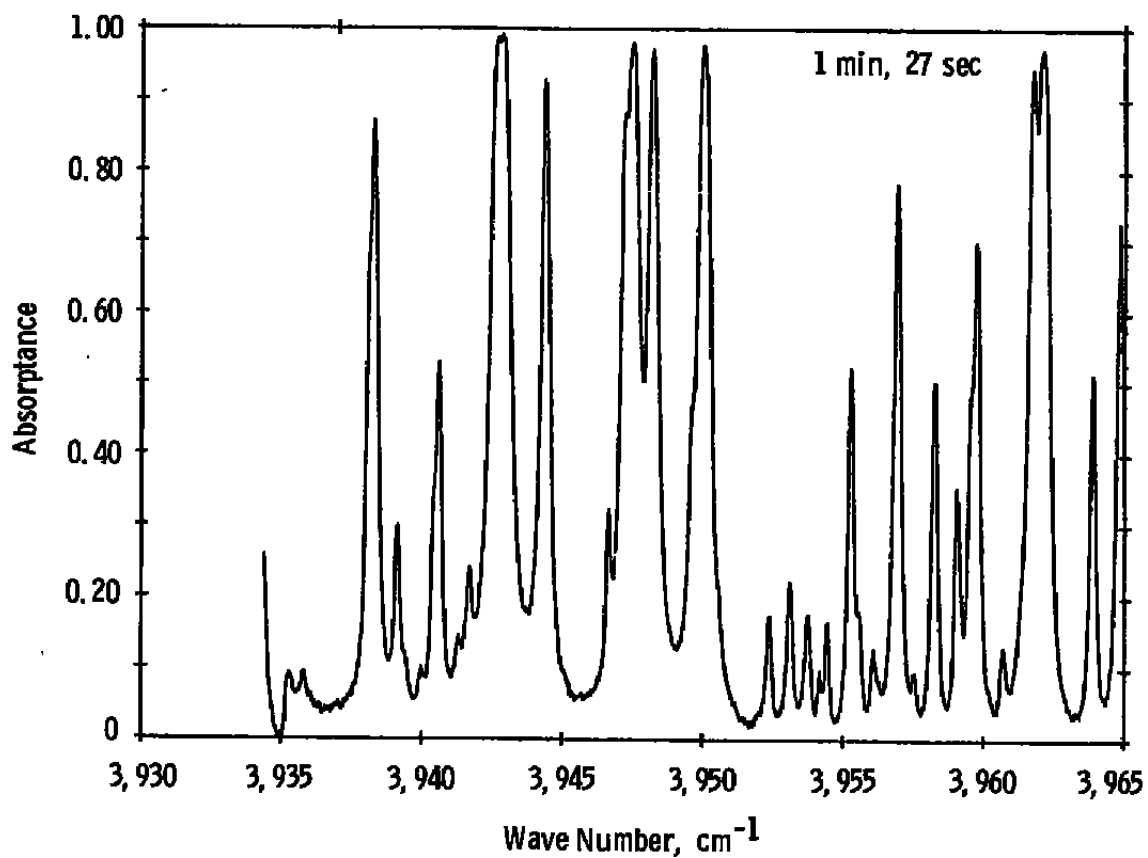
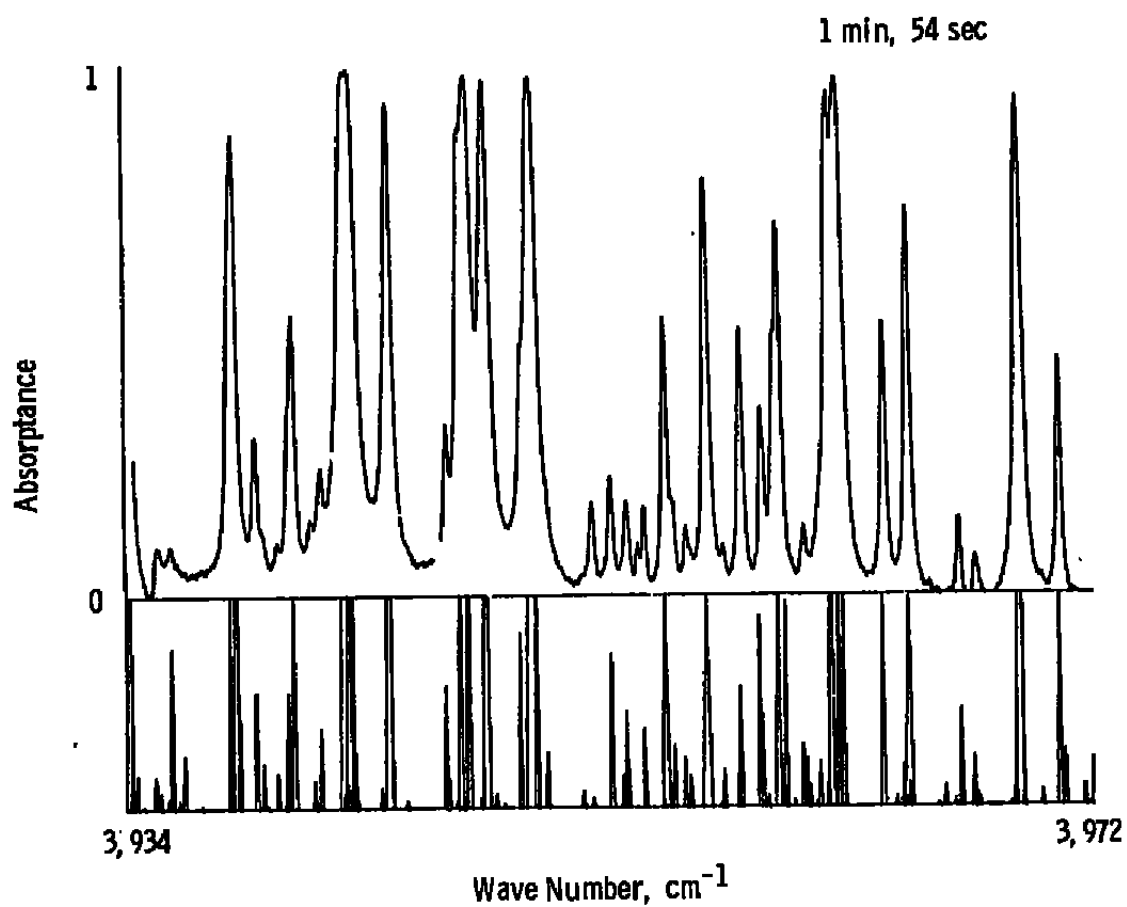
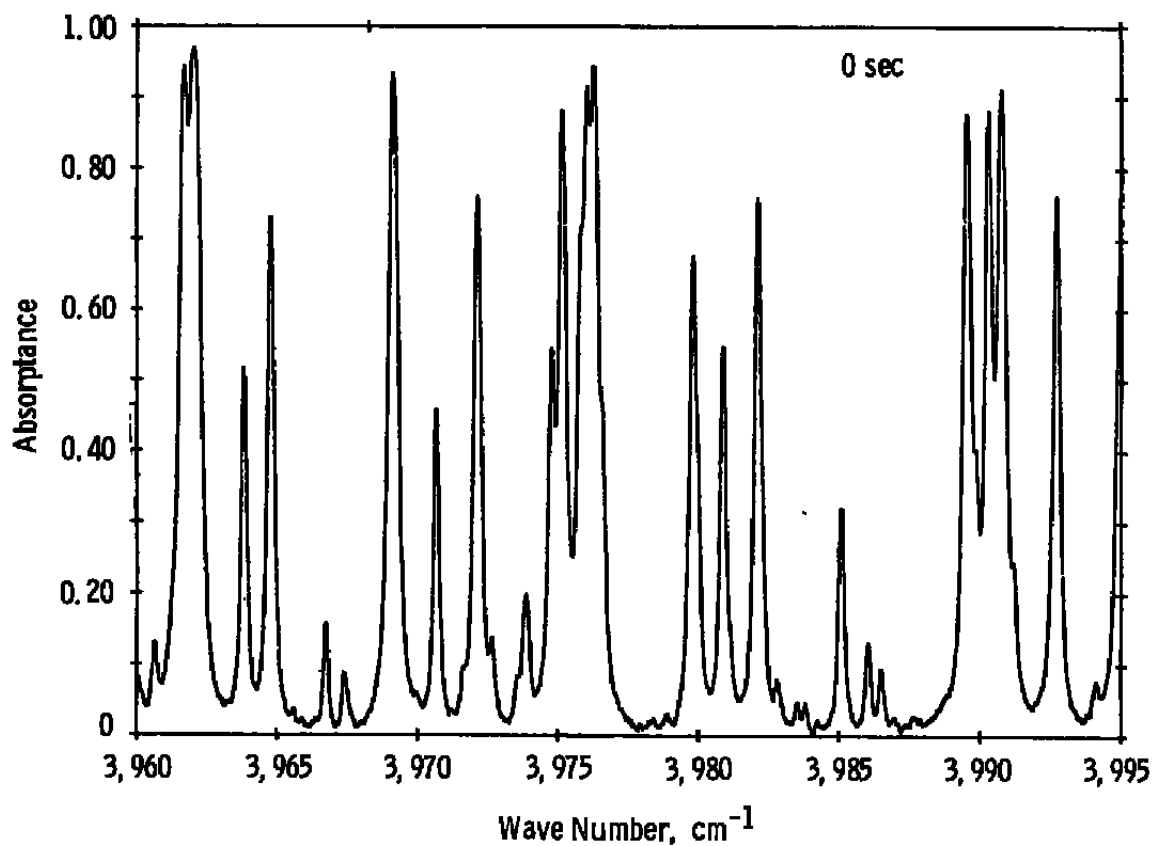


Figure A-21.  $\text{H}_2\text{O}$  absorption in spectral range 3,930 to 3,965  $\text{cm}^{-1}$ , 704K, 280 torr.



**Figure A-22. Comparison of H<sub>2</sub>O spectrum and AFGL line atlas, 3,934 to 3,972 cm<sup>-1</sup>, 704K, 280 torr.**



**Figure A-23.  $\text{H}_2\text{O}$  absorption in spectral range 3,960 to 3,995  $\text{cm}^{-1}$  704 torr, 280 torr.**

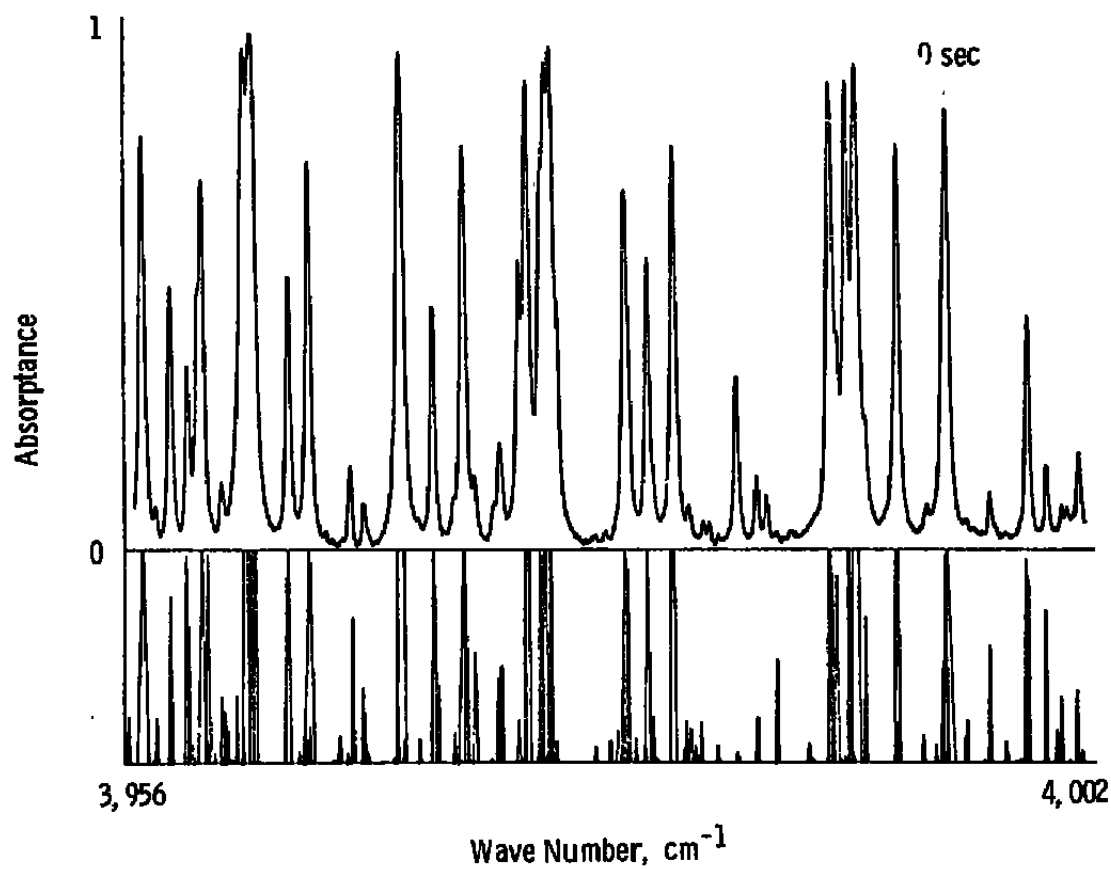


**Figure A-24. Comparison of H<sub>2</sub>O spectrum and AFGL line atlas, 3,956 to 4,002 cm<sup>-1</sup>, 704K, 280 torr.**



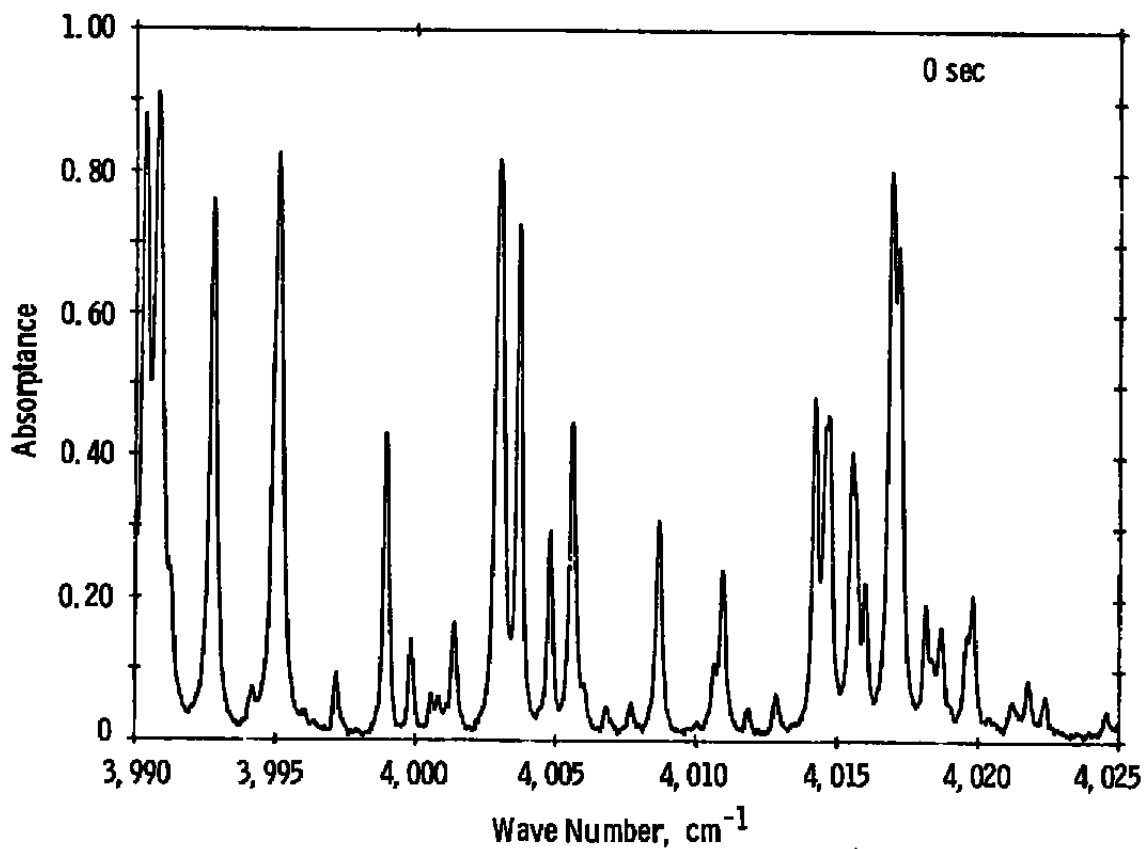
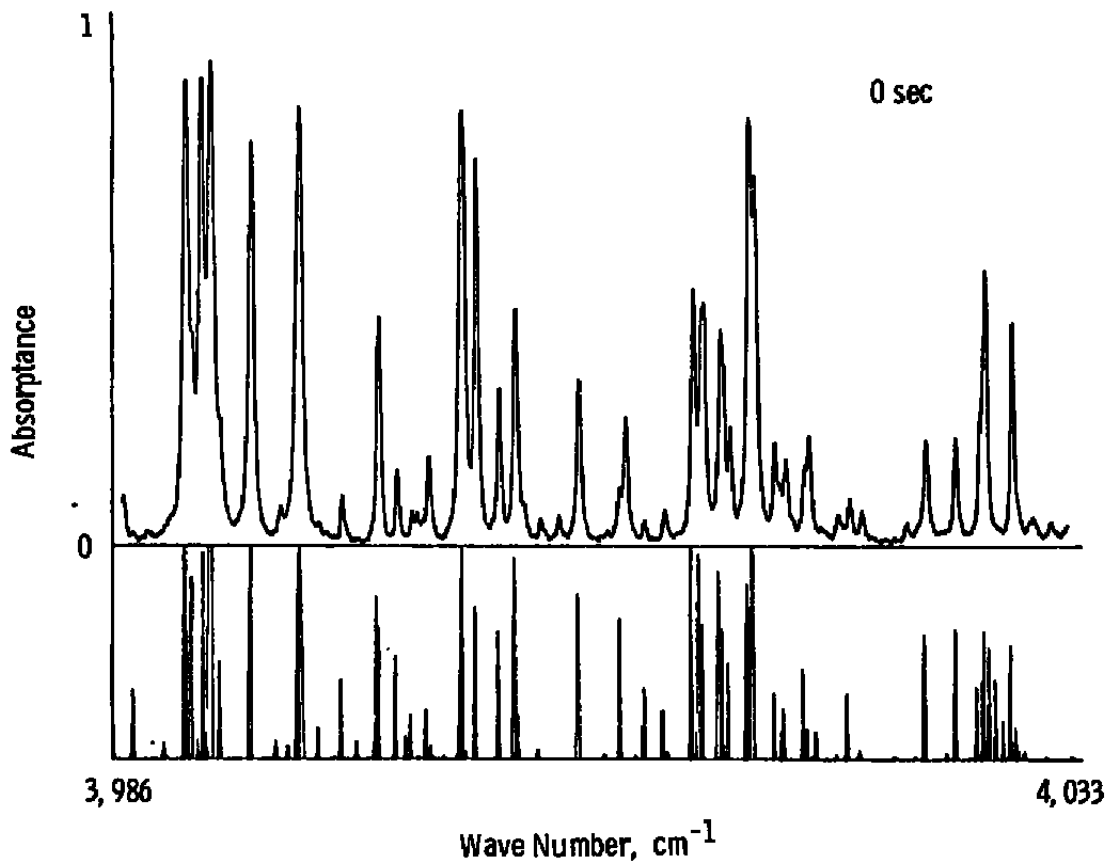


Figure A-25. H<sub>2</sub>O absorption in spectral range 3,990 to 4,025 cm<sup>-1</sup>, 704K, 280 torr.



**Figure A-26. Comparison of  $\text{H}_2\text{O}$  spectrum and AFGL line atlas, 3,986 to 4,033 torr, 704K, 280 torr.**

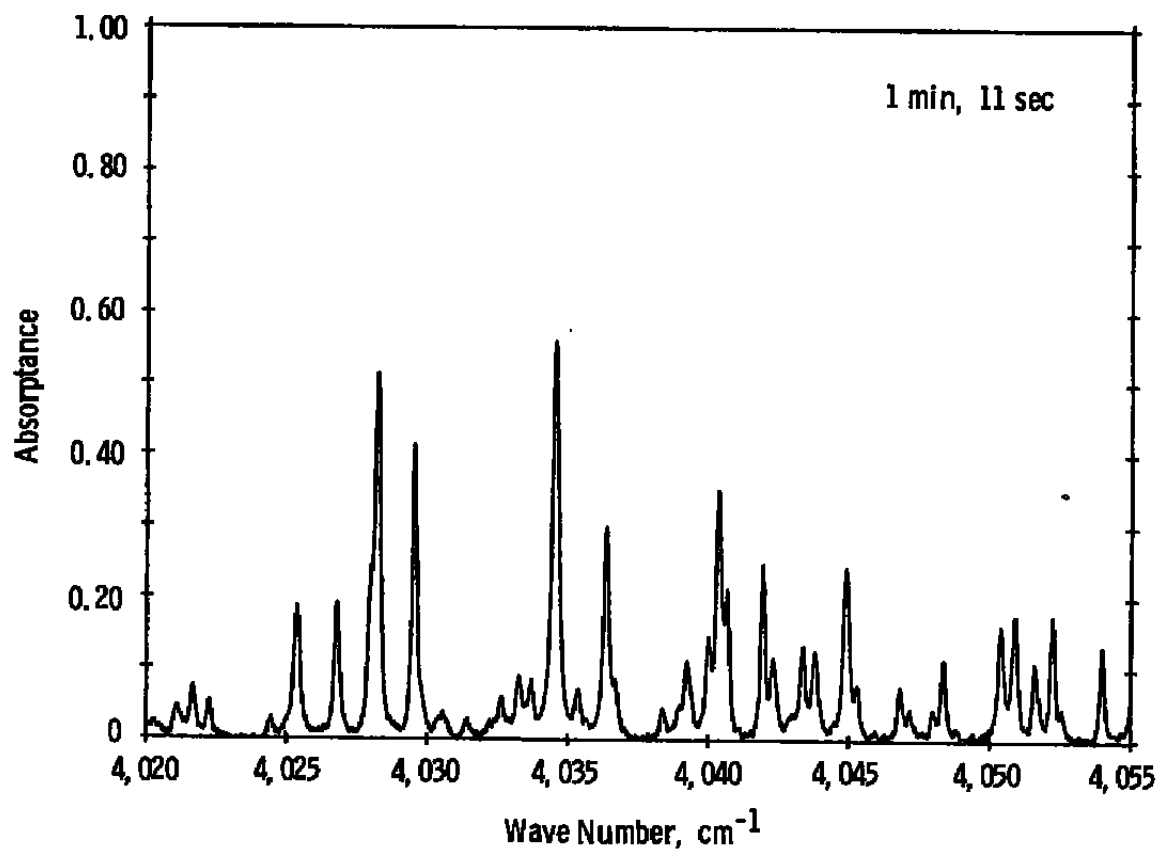
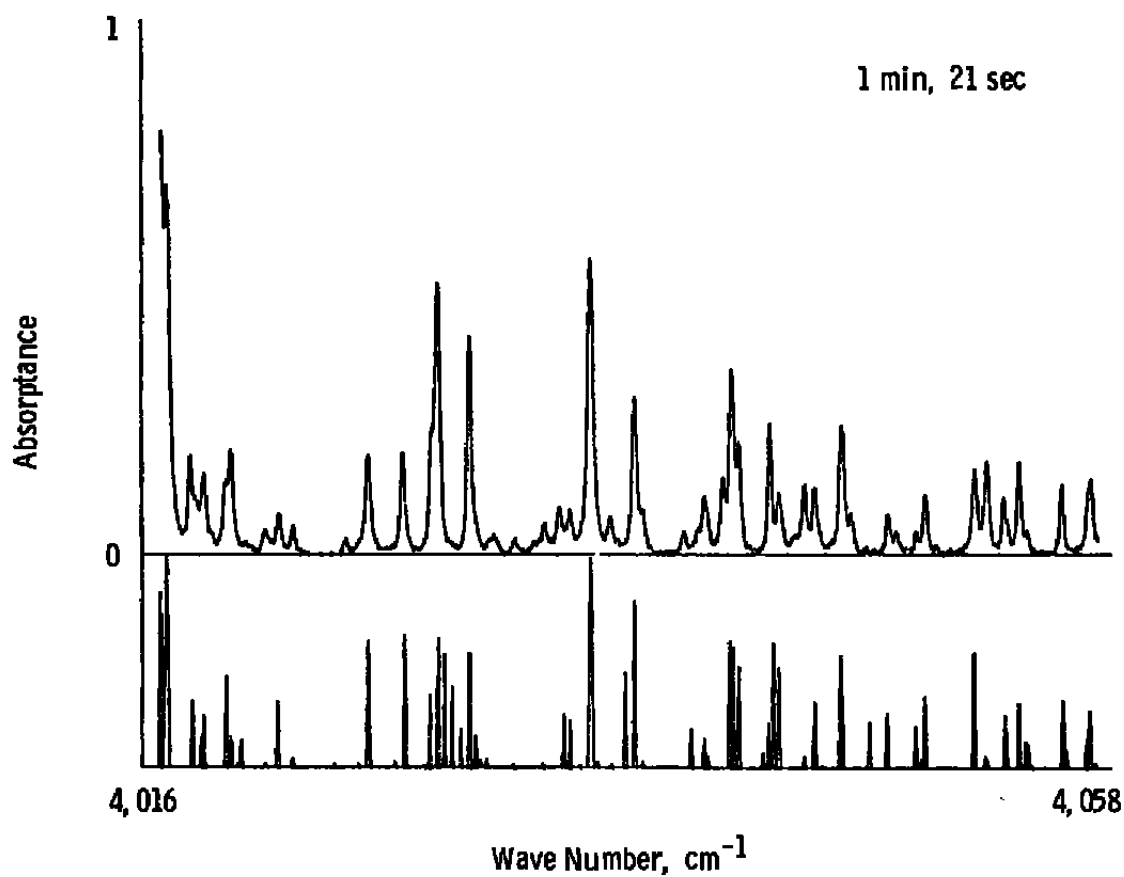
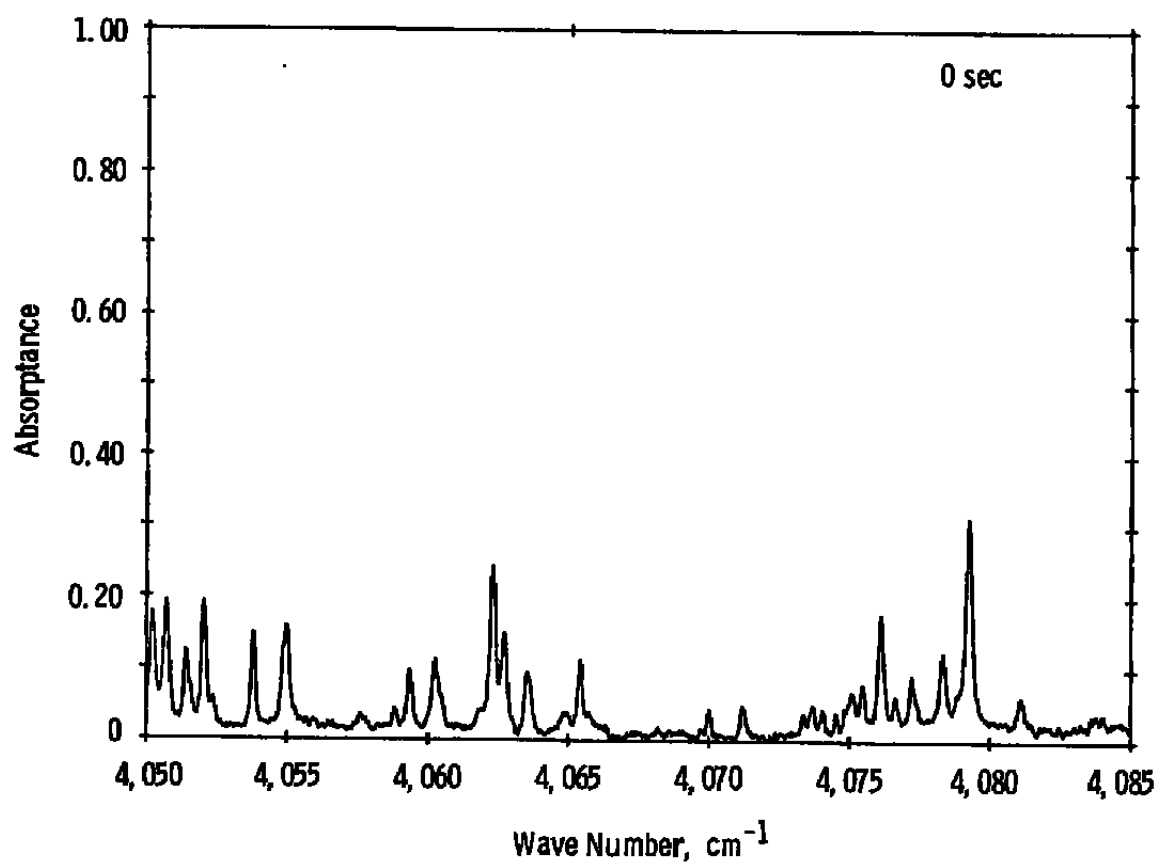


Figure A-27. H<sub>2</sub>O absorption in spectral range 4,020 to 4,055 cm<sup>-1</sup>, 704K, 280 torr.



**Figure A-28. Comparison of H<sub>2</sub>O spectrum and AFGL line atlas, 4,016 to 4,058 cm<sup>-1</sup>, 704K, 280 torr.**



**Figure A-29. H<sub>2</sub>O absorption in spectral range 4,050 to 4,085 cm<sup>-1</sup>, 704K, 280 torr.**

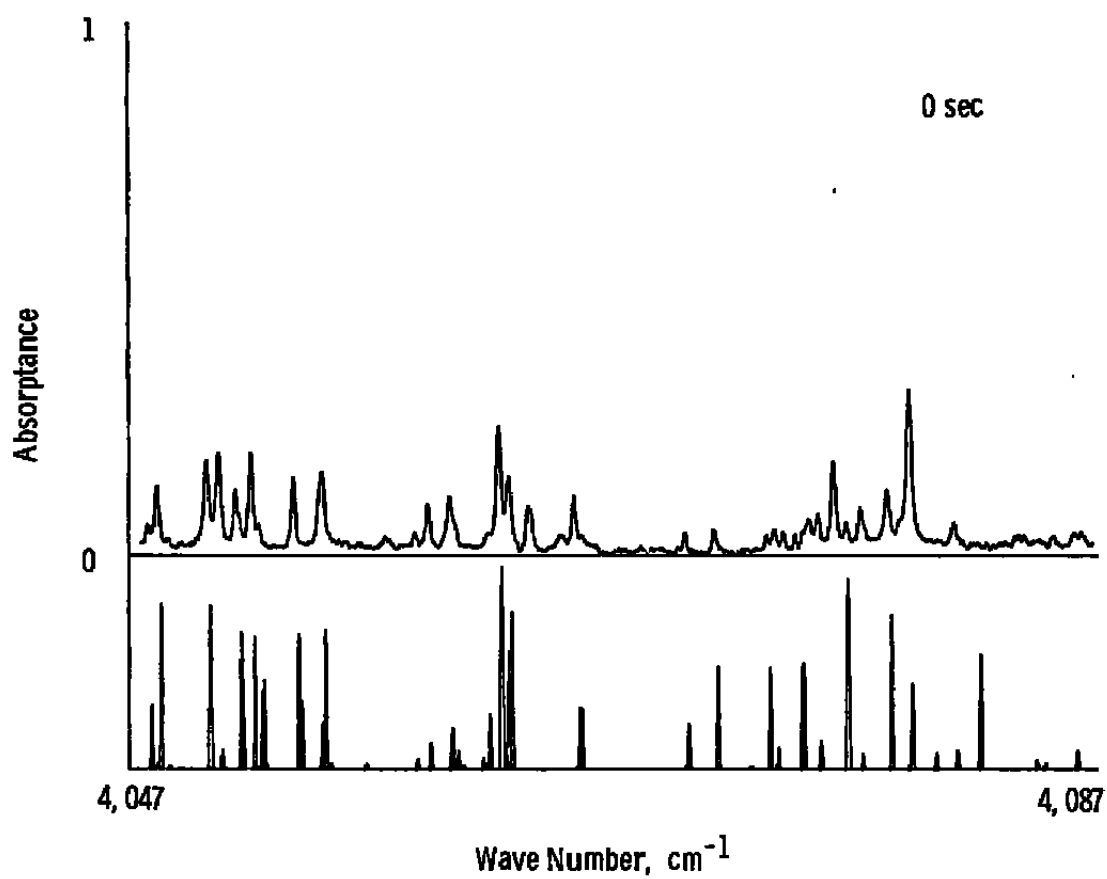


**Figure A-30. Comparison of  $\text{H}_2\text{O}$  spectrum and AFGL line atlas, 4,047 to 4,087  $\text{cm}^{-1}$ , 704K, 280 torr.**

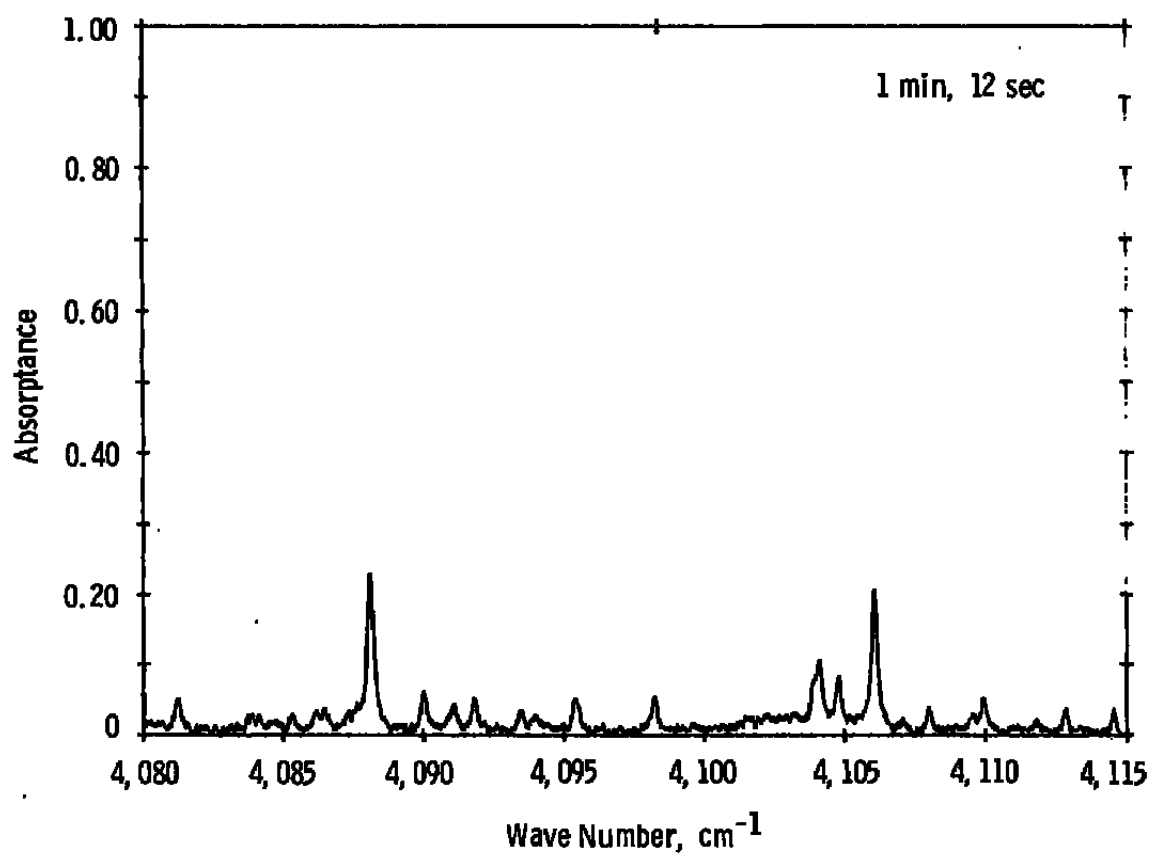
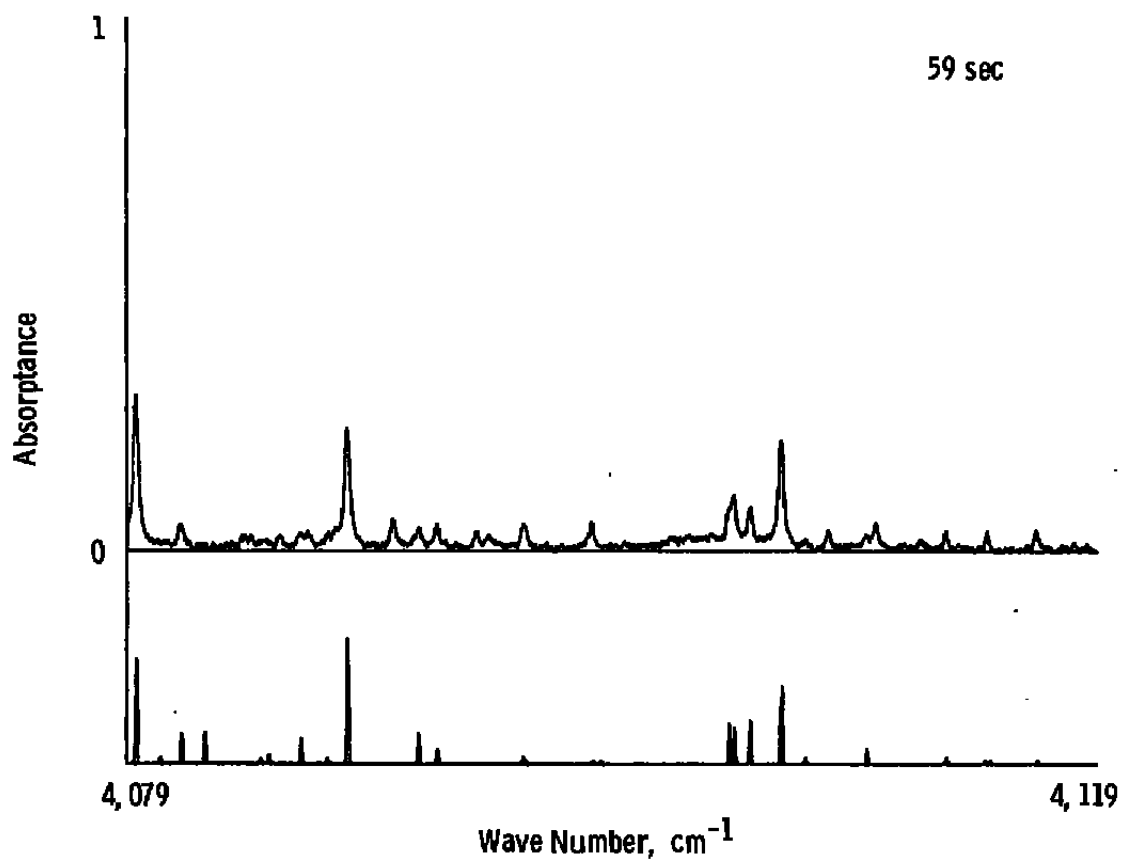


Figure A-31. H<sub>2</sub>O absorption in spectral range 4,080 to 4,115 cm<sup>-1</sup>, 704K, 280 torr.



**Figure A-32. Comparison of H<sub>2</sub>O spectrum and AFGL line atlas, 4,079 to 4,119 cm<sup>-1</sup>, 704K, 280 torr.**



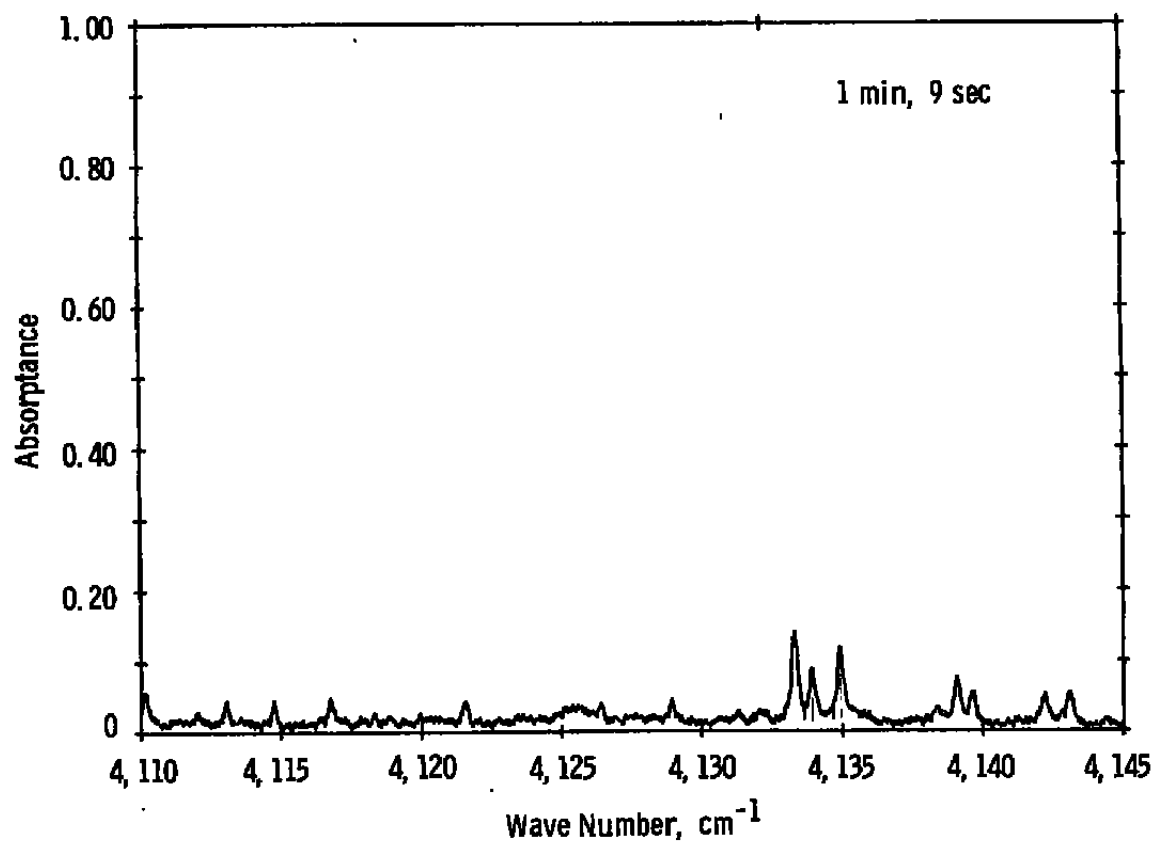
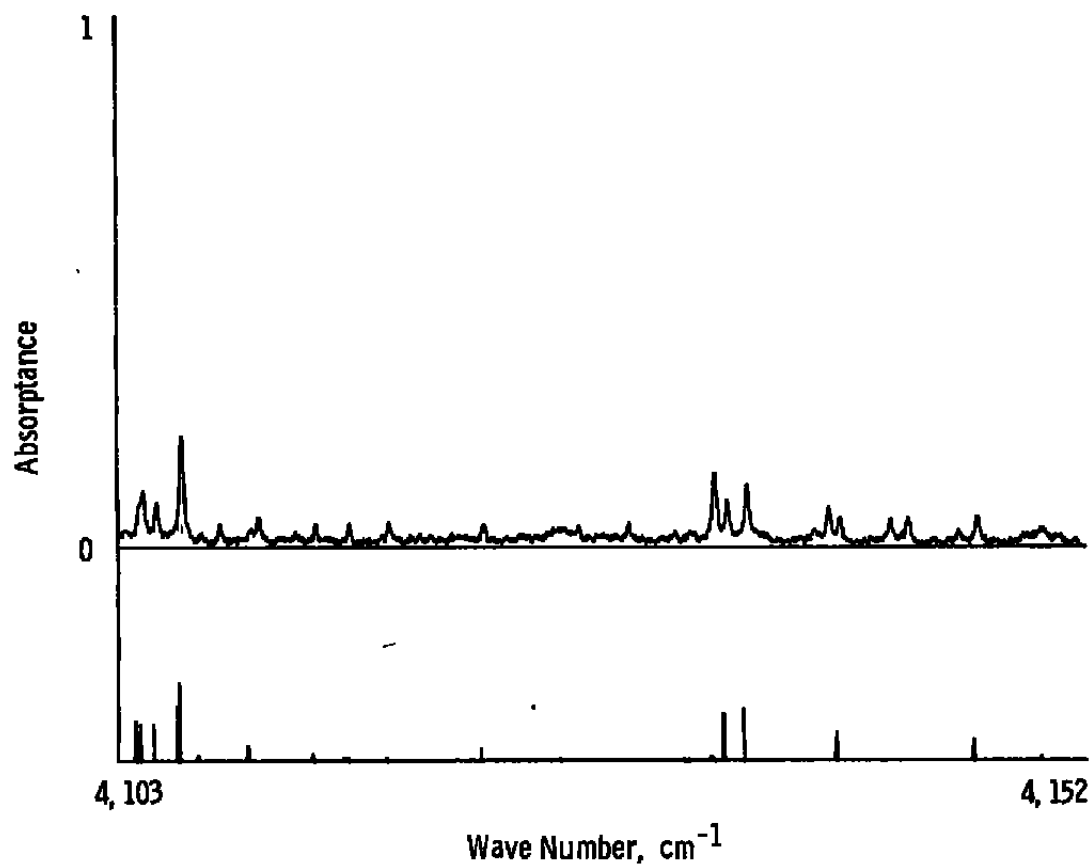


Figure A-33. H<sub>2</sub>O absorption in spectral range 4,110 to 4,145 cm<sup>-1</sup>, 704K, 280 torr.



**Figure A-34. Comparison of  $\text{H}_2\text{O}$  spectrum and AFGL line atlas, 4,103 to 4,152  $\text{cm}^{-1}$ , 704K, 280 torr.**

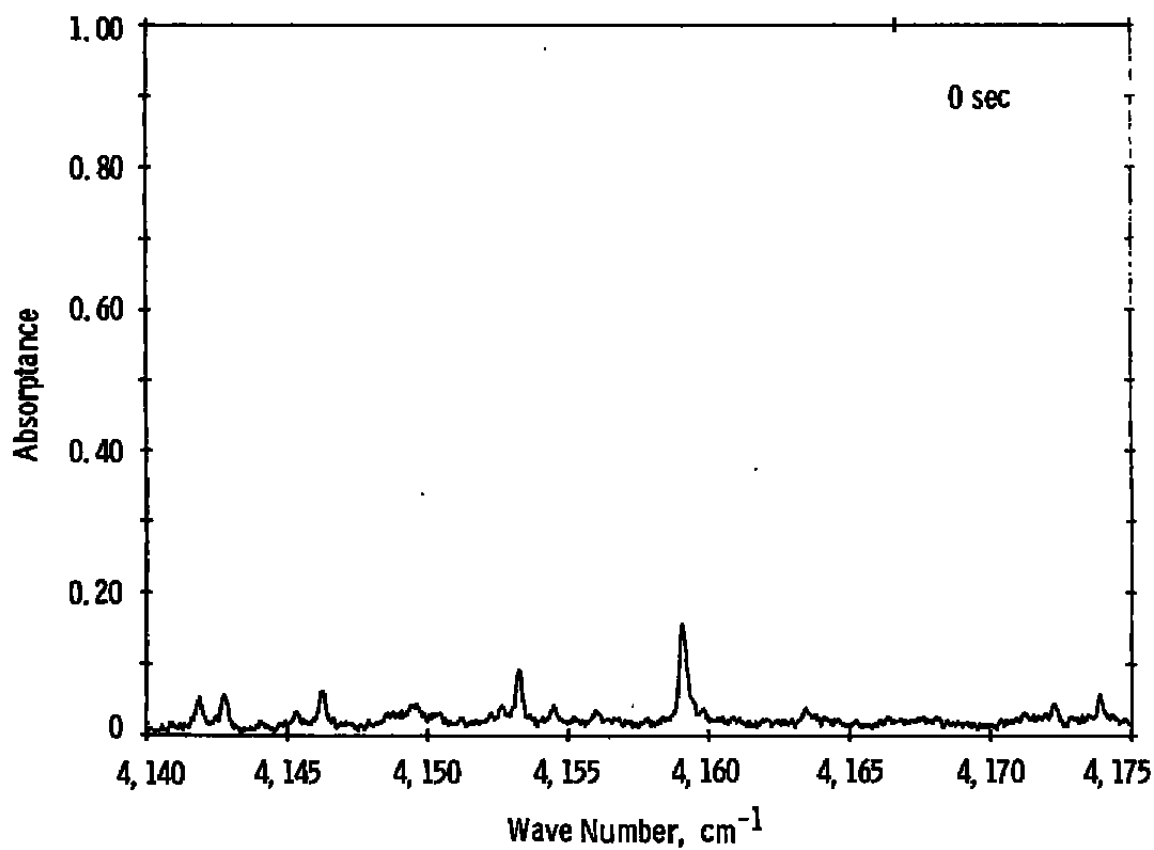
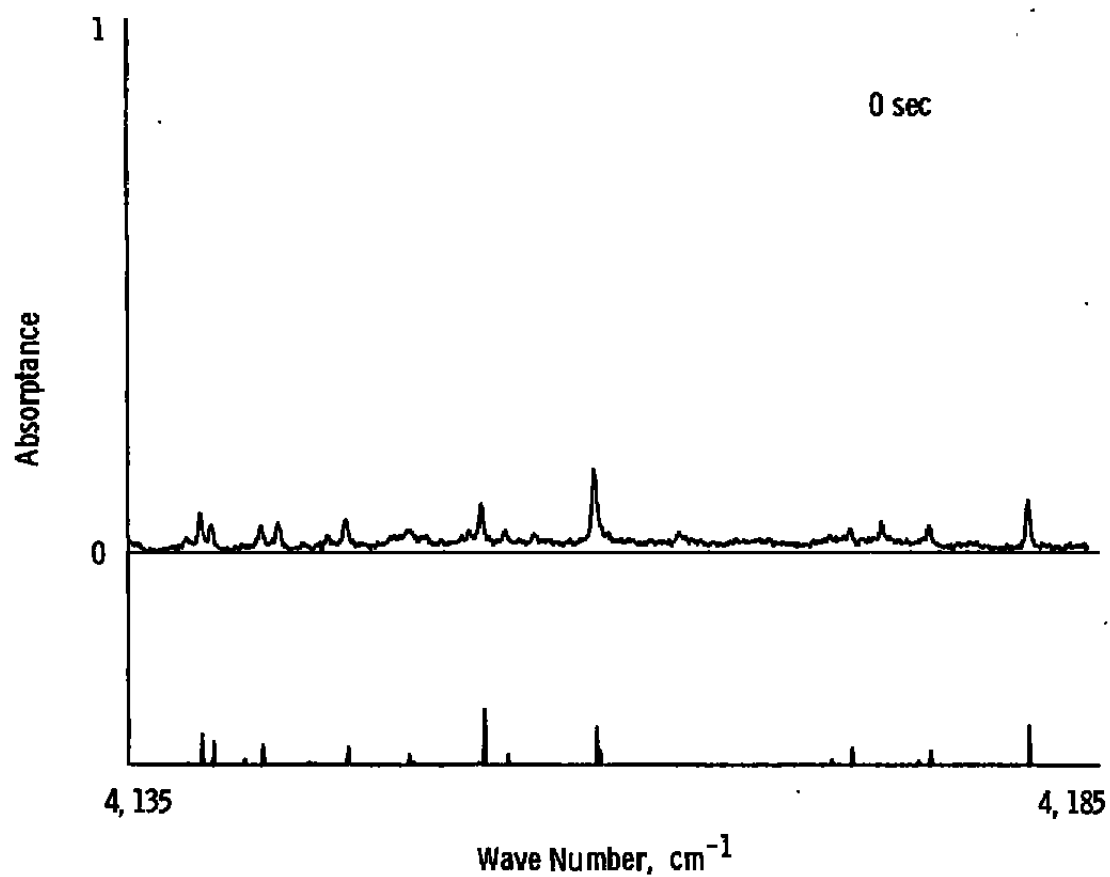
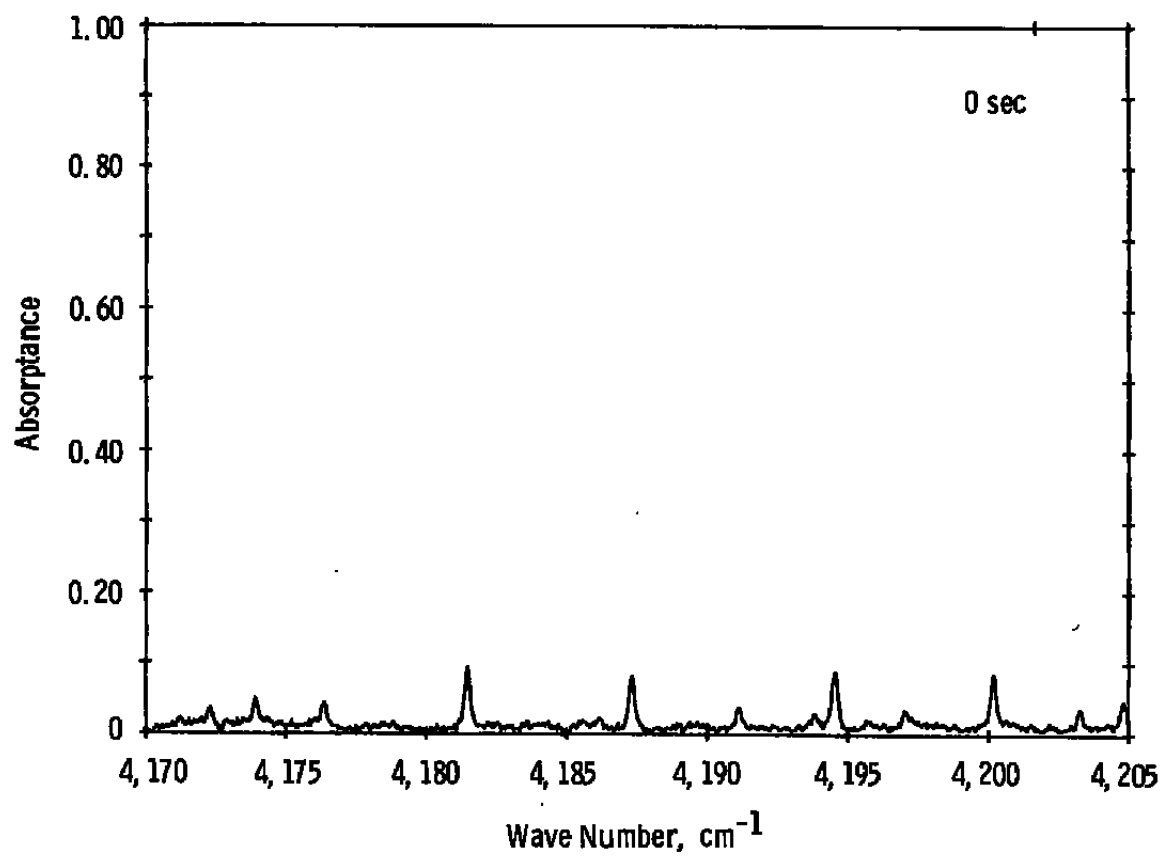


Figure A-35. H<sub>2</sub>O absorption in spectral range 4,140 to 4,175 cm<sup>-1</sup>, 704K, 280 torr.



**Figure A-36. Comparison of H<sub>2</sub>O spectrum and AFGL line atlas, 4,135 to 4,185 cm<sup>-1</sup>, 704K, 280 torr.**



**Figure A-37. H<sub>2</sub>O absorption in spectral range 4,170 to 4,205 cm<sup>-1</sup>, 704K, 280 torr.**

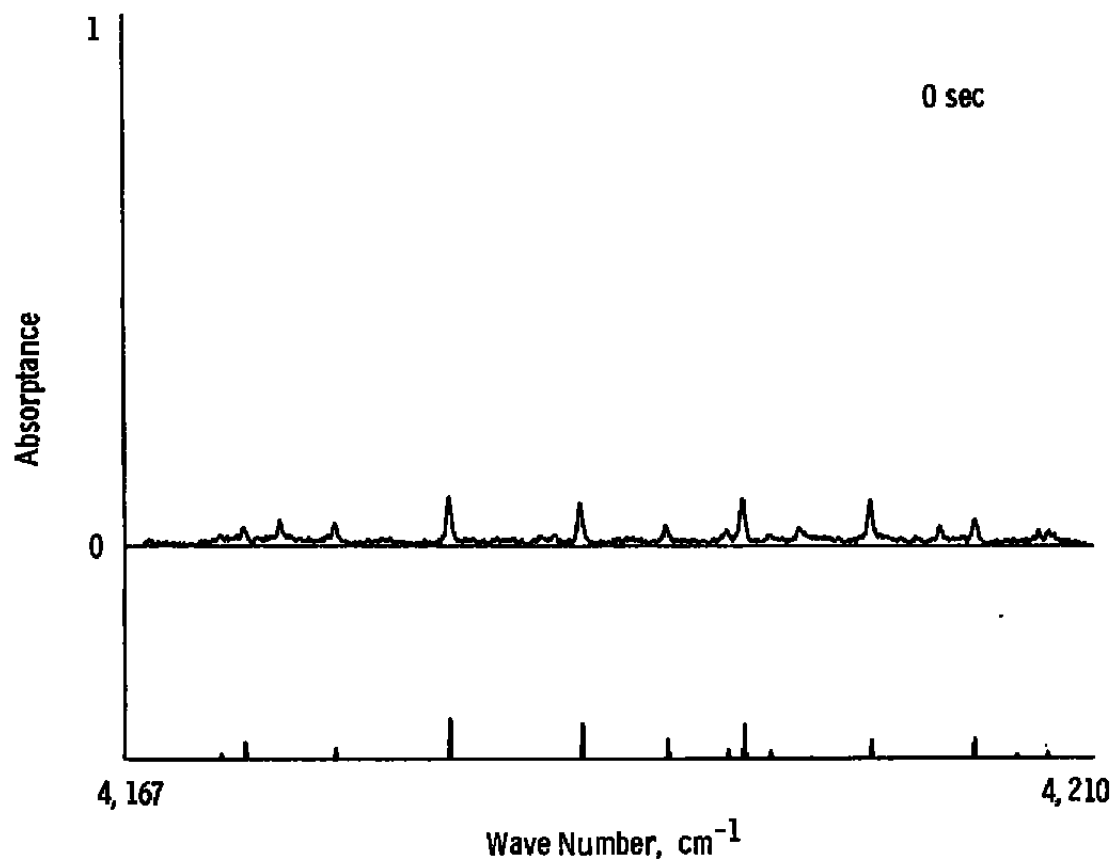


**Figure A-38. Comparison of  $\text{H}_2\text{O}$  spectrum and AFGL line atlas, 4,167 to 4,210  $\text{cm}^{-1}$ , 704K, 280 torr.**

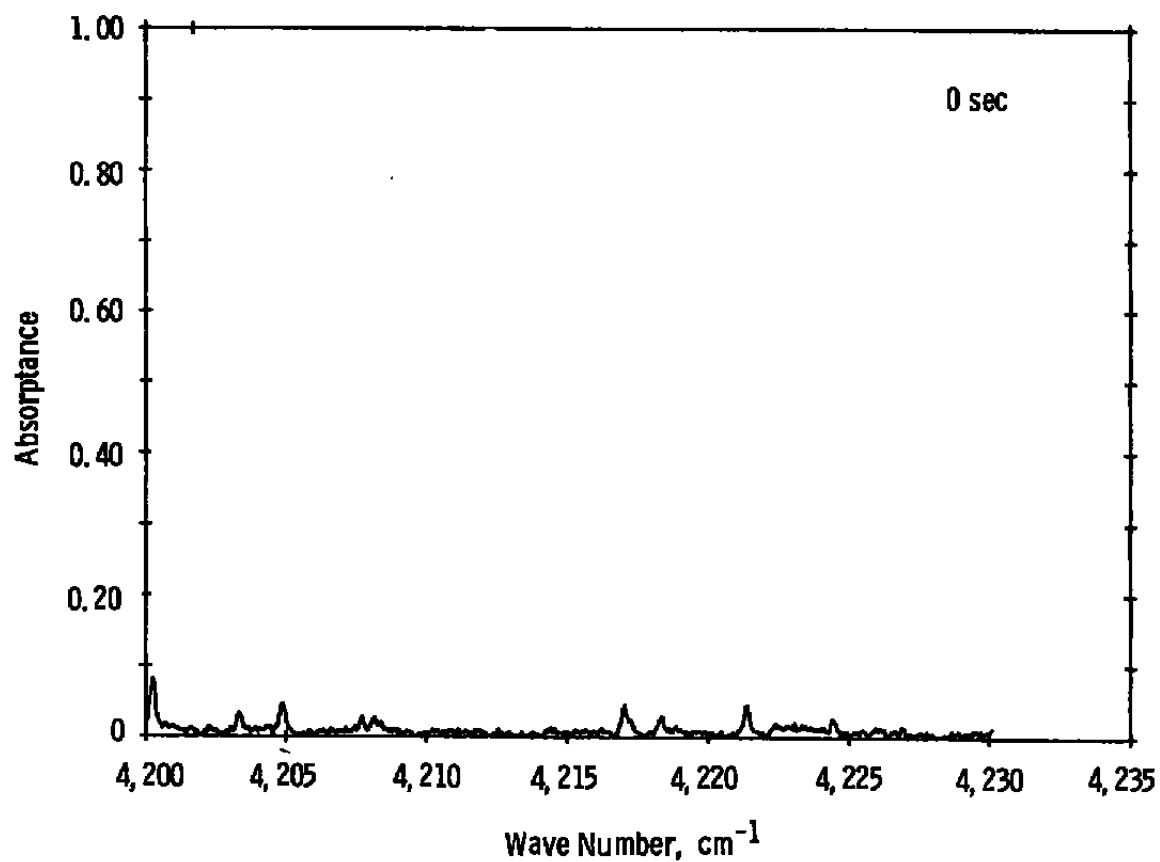


**Figure A-39. H<sub>2</sub>O absorption in spectral range 4,200 to 4,235 cm<sup>-1</sup>, 704K, 280 torr.**

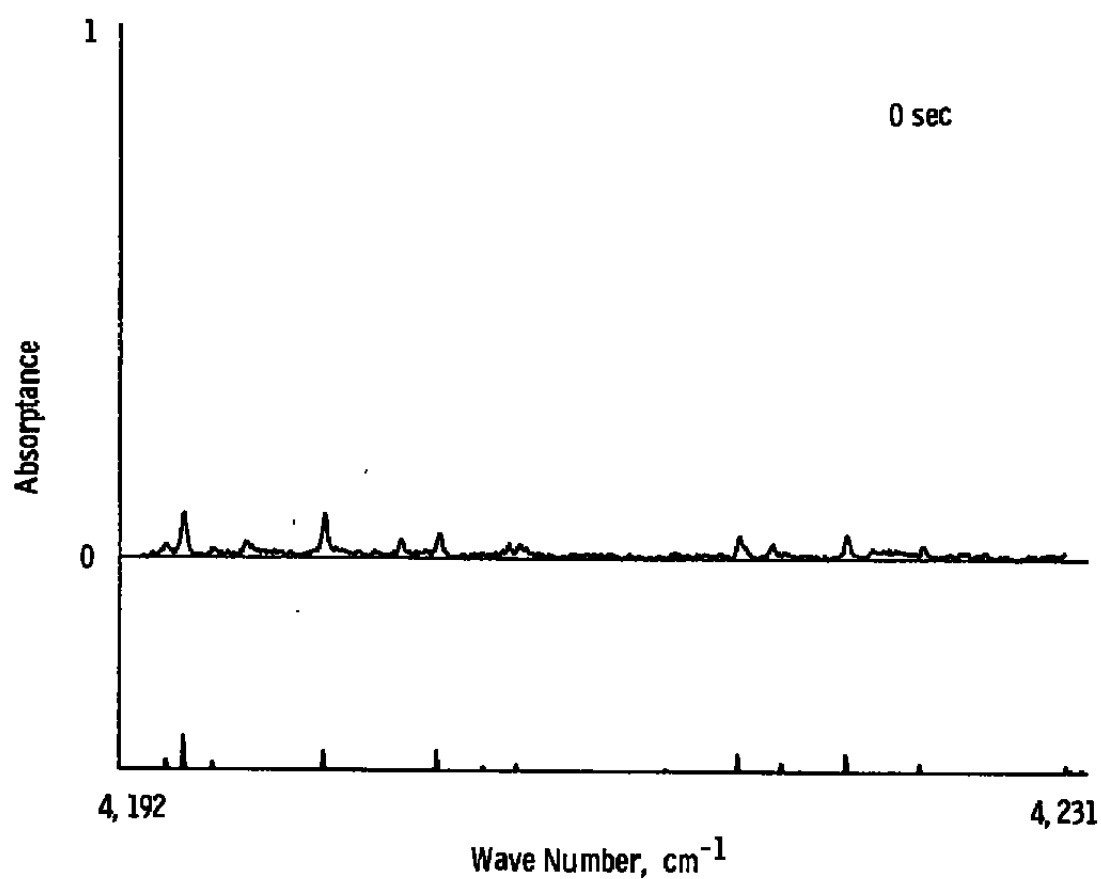


**Figure A-40. Comparison of  $\text{H}_2\text{O}$  spectrum and AFGL line atlas, 4,192 to 4,231 torr, 704K, 280 torr.**



**Table A-1. Experimental Conditions for High-Resolution Spectral Scans**

Resolution:  $0.10 \text{ cm}^{-1}$   
 Scan Rate:  $17 \text{ \AA/min}$  ( $\sim 2 \text{ cm}^{-1}/\text{min}$ )  
 Integration: 1 sec  
 Data Rate: 12 data/drum number  
               ( $\sim 0.014 \text{ cm}^{-1}/\text{datum}$ )  
               (1 drum number =  $\sim 1 \text{ \AA}$ )  
 Cell Length: 15 cm

Run	Pressure (torr)	Temperature (K)	Optical Depth (molecules/cm <sup>2</sup> )	Coverage Wave Number (cm <sup>-1</sup> )	Wavelength ( $\mu\text{m}$ )
H	414	1,002	$5.99 \times 10^{19}$	3,930 - 4,230	2.36 - 2.54
I	280	704	$5.27 \times 10^{19}$	3,930 - 4,260	2.35 - 2.54

## APPENDIX B

### IR SPECTRA DECONVOLUTION

This appendix describes a deconvolution algorithm for restoration of the spectral distribution which was degraded by the instrument function. Preliminary results are shown for a simulation which will be helpful in predicting the performance of the algorithm.

The distortion (broadening) of the true molecular spectrum by the instrument function is described by the integral equation:

$$S(\lambda) = \int h(\lambda, \lambda_0) T(\lambda_0) d\lambda_0 \quad (B-1)$$

where  $S(\lambda)$  is the measured spectrum,  $h(\lambda)$  is the instrument function, and  $T(\lambda)$  is the true spectral distribution. It is generally assumed that the instrument function is shift invariant so that Eq. (B-1) reduces to:

$$S(\lambda) = \int h(\lambda - \lambda_0) T(\lambda_0) d\lambda_0 \quad (B-2)$$

which is the convolution integral. The problem is to recover  $T$  given the measurements and the instrument function. From laboratory measurement, it was determined that the instrument function is approximately Gaussian with full width at half-maximum of 0.10  $\text{cm}^{-1}$  (approximately eight data samples). Furthermore, the signal-to-noise ratio is expected to be approximately 200:1.

An iterative deconvolution algorithm was selected for the following reasons:

1. The algorithm makes no assumptions about the shape of the spectral distribution to be recovered.
2. Improved precision is expected with an increasing number of iterations if the signal-to-noise ratio is high, and if the desired resolution is approximately the same order as the wavelength spacing.
3. The algorithm is computationally efficient, especially if the instrument function is symmetric.

If the assumptions in Eq. (B-2) are not satisfied, or if the instrument function is asymmetric, then other techniques should be considered.

With  $N$  equally spaced measurements available, the integral in Eq. (B-2) is replaced by the sum:

$$S_k = \Delta\lambda \sum_{i=1}^N h_{ki} \cdot T_i \text{ for } k = 1, \dots, N \quad (\text{B-3})$$

Where  $S_k$  is the  $k^{\text{th}}$  measurement,  $\Delta\lambda$  is the wavelength spacing, and  $T_i$  is the  $i^{\text{th}}$  sample of the true spectral distribution. Hence, the deconvolution procedure reduces to a system of  $N \times N$  linear equations. Iterative improvement of the solution is obtained by computing the residual after each iteration and applying an additive correction. In the algorithm used here, a multiplicative factor to accelerate convergence was also used.

The first procedure used to test and predict the performance of the algorithm was to recover a known spectral distribution which was degraded by the instrument function. In this case, the measurements correspond to the Gaussian function (i.e., recovery of a Dirac delta function is desired). The printer plots on the following pages show the results of the simulation for the cases of 1, 2, 5, and 10 iterations. After each iteration, it is expected that the output peak value will increase and that the FWHM will decrease (i.e., approaching a delta function). Table B-1 shows the results. The plots and table show an increase in peak value and decrease in spectral width as the number of iterations increases. However, the peak is a long way from infinity and the width is much larger than zero. Also, it is worth noting the side lobes which become more pronounced as the iterations increase.

Actual data reduction for the spectral measurements will be the deconvolution of a true spectral absorption line which is equal to or greater than the instrument function. As such, the deconvolution will be a minor correction to the measured spectrum. The deconvolution of a delta function is, however, a good test of the deconvolution algorithm and provides a first-cut quantification of its usefulness.

It is recommended that the following additional analyses be performed:

1. Repeat the simulation above when the spacing between adjacent spectral lines is of the order of the instrument function half-width.
2. Convolve Lorentzian functions (with known FWHM and peak values) with the Gauss instrument function. Use the deconvolution technique to recover the Lorentzian shapes. Repeat with overlapping spectral lines.

3. Repeat (1) and (2) above with noise added. Determine if the noise will shift the peak position or alter the line width. Furthermore, determine if a relationship exists between the noise and the number of useful iterations (i.e., determine if the solution will become worse with increasing number of iterations).
4. Modify the algorithm to incorporate any *a priori* information which may be useful (i.e., can one utilize the Lorentzian line shape for pressure broadening as well as the Gaussian instrument function to resolve overlapping spectral lines).

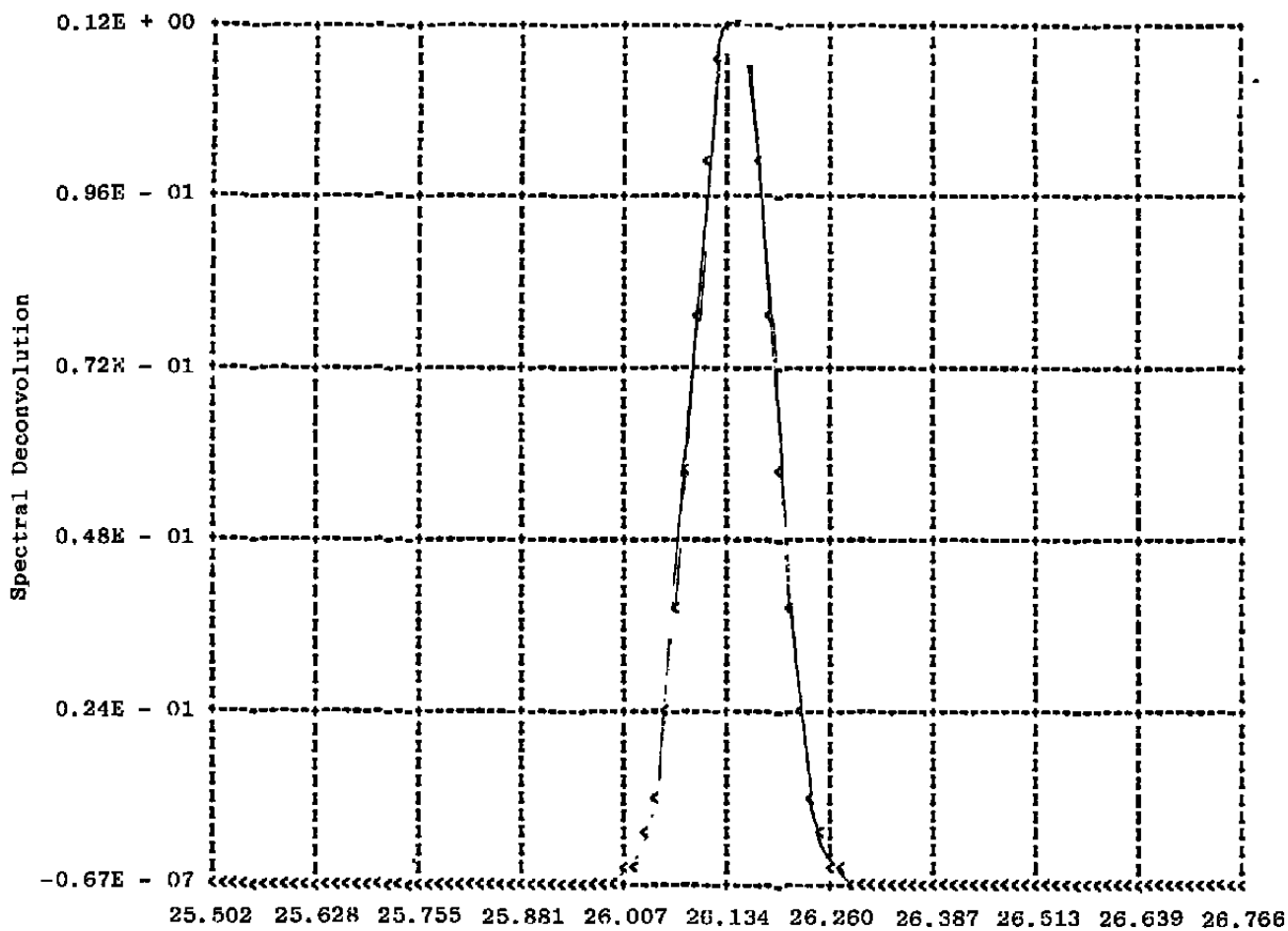
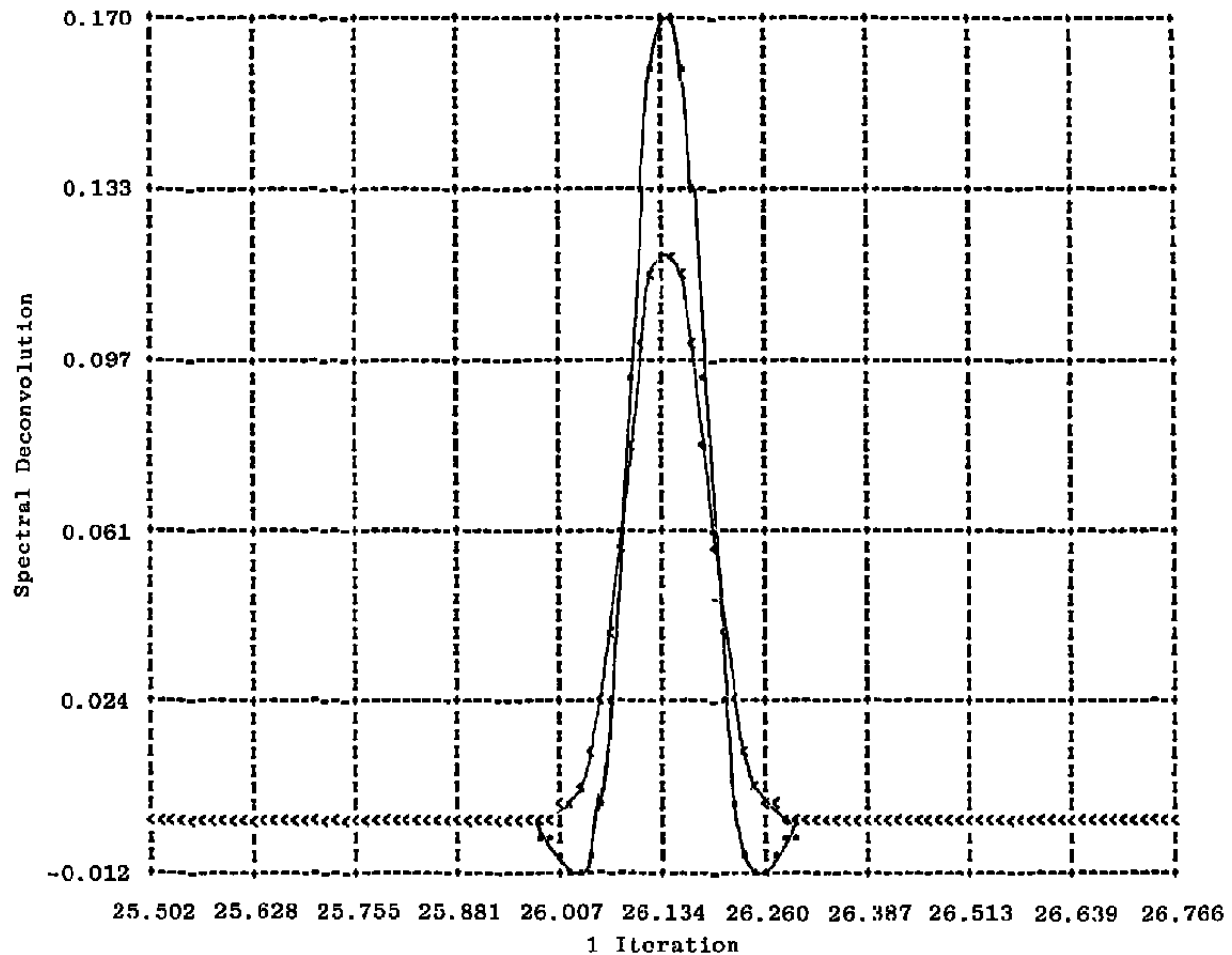
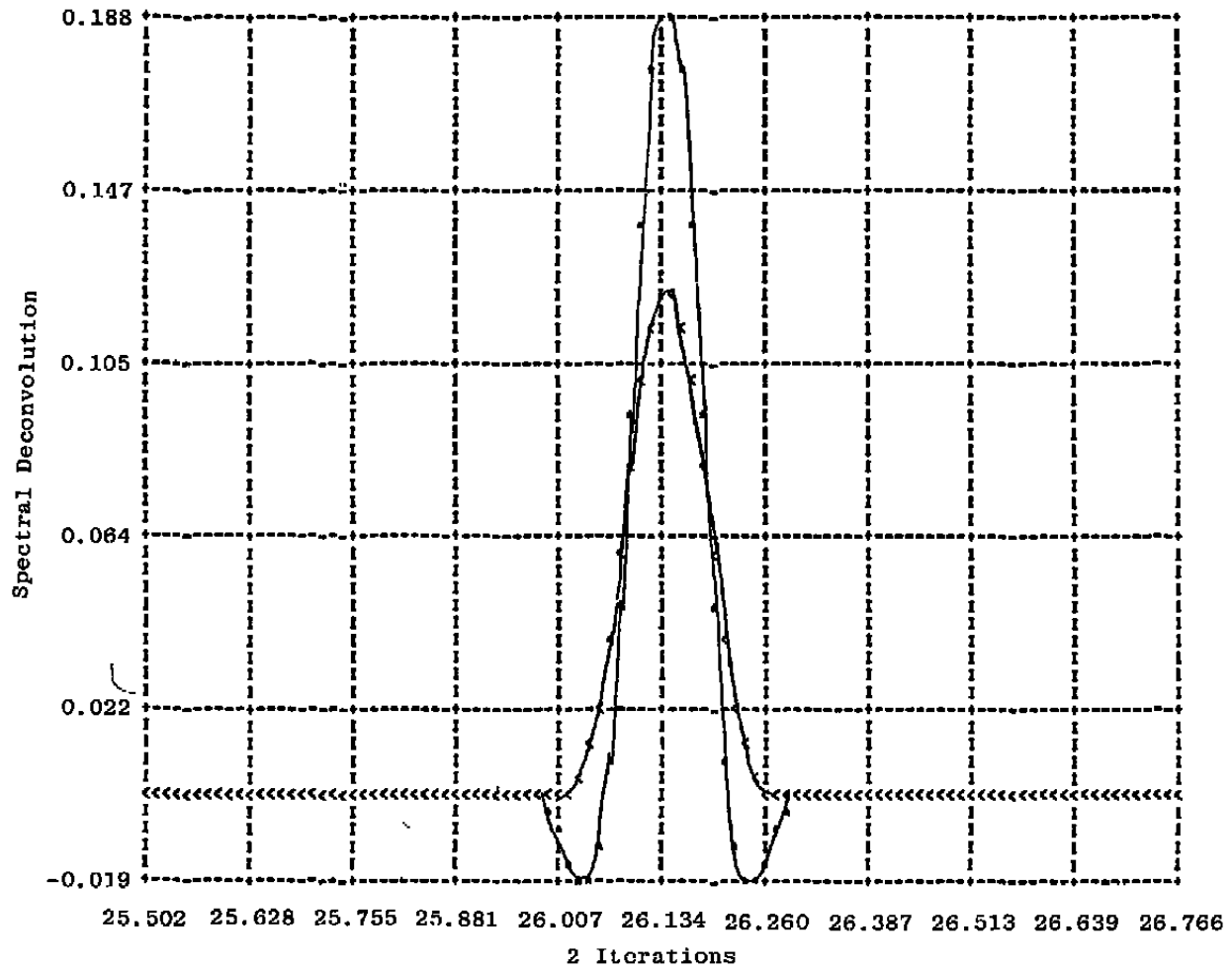


Figure B-1. Gaussian instrument function, FWHM = 0.1.



**Figure B-2. Comparison of Instrument degraded and theoretical line shape, 1 iteration.**



**Figure B-3. Comparison of instrument degraded and theoretical line shape, 2 iterations.**

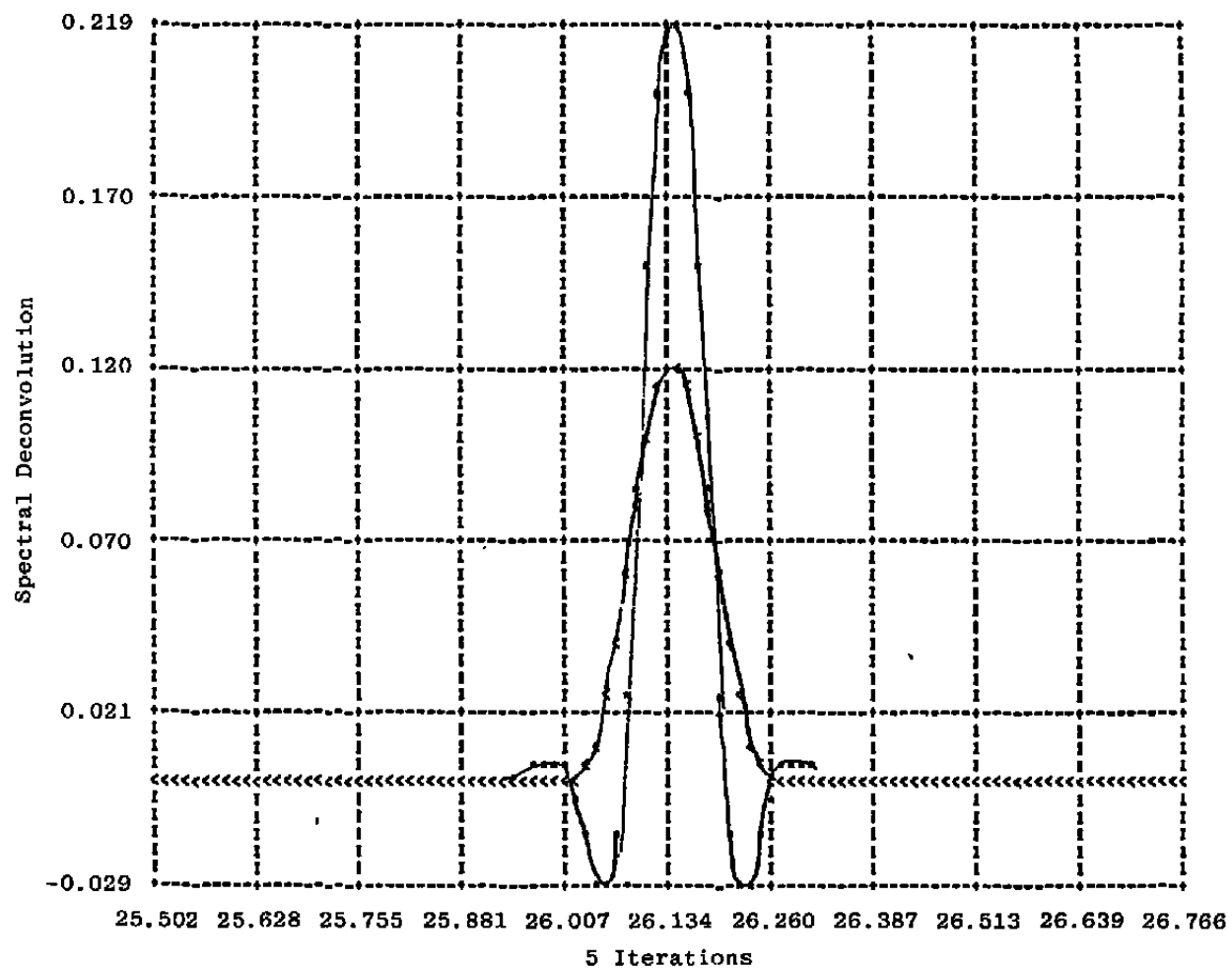


**Figure B-4. Comparison of instrument degraded and theoretical line shape, 5 iterations.**



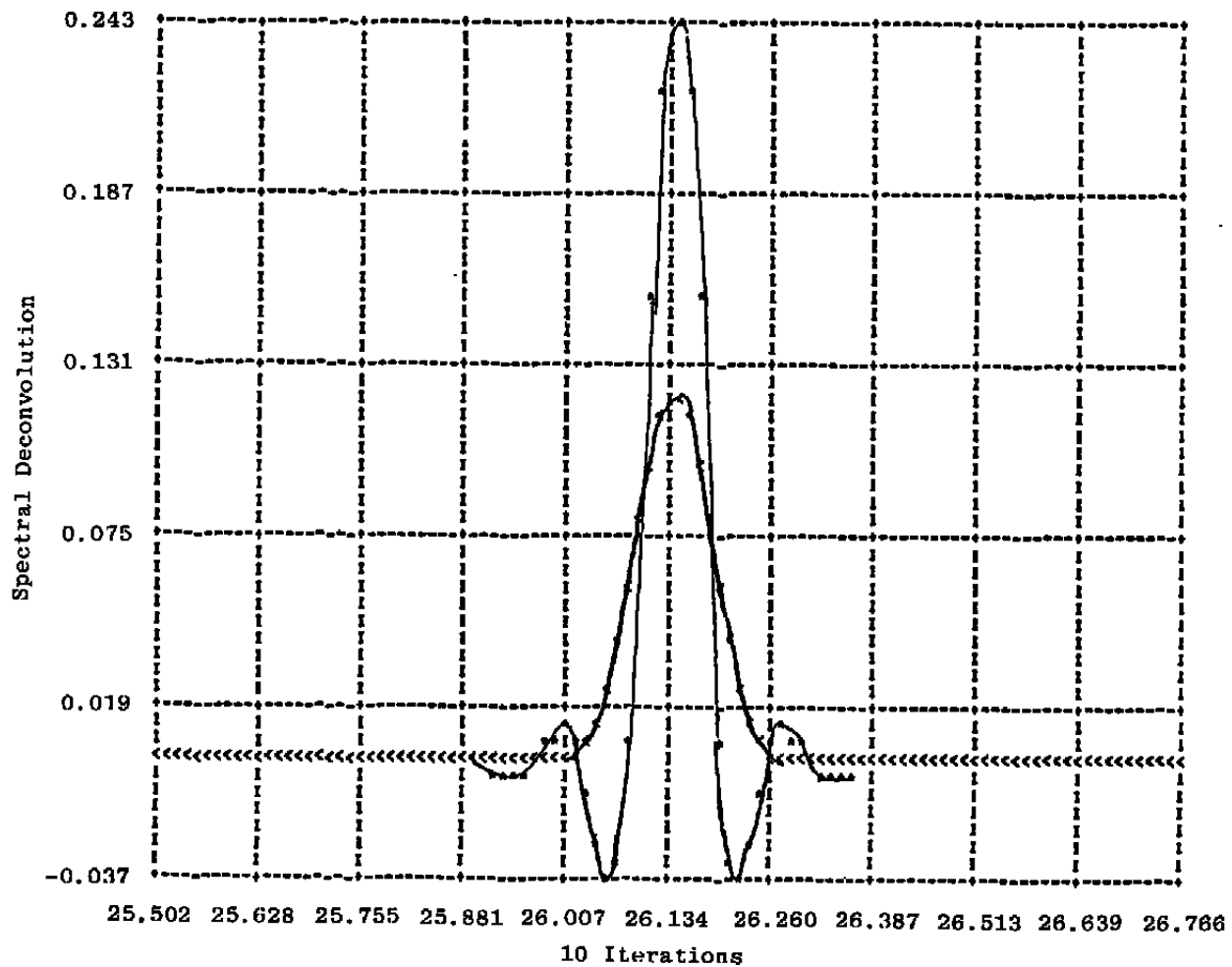


Figure B-5. Comparison of instrument degraded and theoretical line shape, 10 iterations.

**Table B-1. Test the Iterative Deconvolution Algorithm  
with Gaussian Instrument Function as Data**

[Gaussian FWHM =  $0.1 \text{ cm}^{-1}$  (8 counts),  
Gaussian peak value = 0.12]

<u>Iterations</u>	<u>Output Peak Value</u>	<u>Output FWHM (to the nearest sample)</u>	<u>Approximate Improvement Factor on FWHM</u>
1	0.170	7	1.1
2	0.188	6	1.3
5	0.219	5	1.6
10	0.243	5	1.6